

## AN INTERMEDIATE LUMINOSITY TRANSIENT IN NGC 300: THE ERUPTION OF A DUST-ENSHROUDED MASSIVE STAR

E. BERGER<sup>1</sup>, A. M. SODERBERG<sup>1,2</sup>, R. A. CHEVALIER<sup>3</sup>, C. FRANSSON<sup>4</sup>, R. J. FOLEY<sup>1,5</sup>, D. C. LEONARD<sup>6</sup>, J. H. DEBES<sup>7</sup>,  
A. M. DIAMOND-STANIC<sup>8</sup>, A. K. DUPREE<sup>1</sup>, I. I. IVANS<sup>9</sup>, J. SIMMERER<sup>10</sup>, I. B. THOMPSON<sup>9</sup>, C. A. TREMONTI<sup>8</sup>

Draft version October 29, 2018

### ABSTRACT

We present multi-epoch high-resolution optical spectroscopy, UV/radio/X-ray imaging, and archival *Hubble* and *Spitzer* observations of an intermediate luminosity optical transient recently discovered in the nearby galaxy NGC 300. We find that the transient (NGC 300 OT2008-1) has a peak absolute magnitude of  $M_{\text{bol}} \approx -11.8$  mag, intermediate between novae and supernovae, and similar to the recent events M85 OT2006-1 and SN 2008S. Our high-resolution spectra, the first for this event, are dominated by intermediate velocity ( $\sim 200 - 1000$  km s<sup>-1</sup>) hydrogen Balmer lines and Ca II emission and absorption lines that point to a complex circumstellar environment, reminiscent of the yellow hypergiant IRC+10420. In particular, we detect broad Ca II H&K absorption with an asymmetric *red* wing extending to  $\sim 10^3$  km s<sup>-1</sup>, indicative of gas infall onto a massive and relatively compact star (blue supergiant or Wolf-Rayet star); an extended red supergiant progenitor is unlikely. The origin of the inflowing gas may be a previous ejection from the progenitor or the wind of a massive binary companion. The low luminosity, intermediate velocities, and overall similarity to a known eruptive star indicate that the event did not result in a complete disruption of the progenitor. We identify the progenitor in archival *Spitzer* observations, with deep upper limits from *Hubble* data. The spectral energy distribution points to a dust-enshrouded star with a luminosity of about  $6 \times 10^4 L_{\odot}$ , indicative of a  $\sim 10 - 20 M_{\odot}$  progenitor (or binary system). This conclusion is in good agreement with our interpretation of the outburst and circumstellar properties. The lack of significant extinction in the transient spectrum indicates that the dust surrounding the progenitor was cleared by the outburst. We thus predict that the progenitor should be eventually visible with *Hubble* if the transient event marks an evolutionary transition to a dust-free state, or with *Spitzer* if the event marks a cyclical process of dust formation.

*Subject headings:* stars:evolution — stars:mass loss — stars:circumstellar matter — stars:winds, outflows

### 1. INTRODUCTION

In recent years dedicated searches and serendipitous discoveries have uncovered several optical transients with luminosities intermediate between the well-studied classes of nova eruptions ( $M \sim -8$  mag) and supernova (SN) explosions ( $M \sim -17$  mag). As can be expected from the wide gap in luminosity, these intermediate luminosity optical transients (hereafter, ILOTs<sup>11</sup>) appear to be diverse in their properties

and origins. Some have been classified as low luminosity core-collapse SNe, with inferred energies and <sup>56</sup>Ni masses that are at least an order of magnitude below typical SN events (e.g., Pastorello et al. 2004). Others, sometimes initially classified as type IIn SNe, have been subsequently tagged with the catch-all designation of “SN impostors” (e.g., Van Dyk et al. 2000), that includes events resembling luminous blue variable (LBV) eruptions. Finally, a small number of somewhat dimmer events have been recently grouped under the proposed name “luminous red novae” (LRNe; Kulkarni et al. 2007), based on their red optical colors; the origin of LRNe and their relation to each other remain unclear. Overall, the various groupings have been subject to debate, and there is no clear agreement about the nature of individual objects or the degree of overlap between the various designations.

Equally important, the connection between the different types of events and different classes of progenitors remains unclear. For example, some LBV eruptions have been initially classified as SNe (e.g., SNe 1961V and 1954J; Goodrich et al. 1989; Van Dyk et al. 2005). Similarly, the progenitor of the recent event SN 2008S, which was detected in archival *Spitzer Space Telescope* images, has been argued to be an extreme AGB star (Prieto et al. 2008; Thompson et al. 2008) or an LBV (Smith et al. 2008). The nature of the event itself is also unclear, with claims of a low mass electron-capture SN (Thompson et al. 2008) and an LBV-like outburst (Smith et al. 2008). The recent event M85 OT2006-1, and the possibly related eruptive object V838 Mon, have been speculated to possibly result from stellar mergers (Munari et al. 2002; Soker & Tylenda 2006; Kulkarni et al. 2007), but other possibilities have been proposed such as a low-luminosity SN for M85 OT2006-1 (Pastorello et al. 2007), and an AGB

<sup>1</sup> Harvard-Smithsonian Center for Astrophysics, 60 Garden Street, Cambridge, MA 02138

<sup>2</sup> Hubble Fellow

<sup>3</sup> Department of Astronomy, University of Virginia, P.O. Box 400325, Charlottesville, VA 22904-4325

<sup>4</sup> Department of Astronomy, Stockholm University, AlbaNova, SE-106 91 Stockholm, Sweden

<sup>5</sup> Clay Fellow

<sup>6</sup> Department of Astronomy, San Diego State University, PA-210, 5500 Campanile Drive, San Diego, CA 92182-1221

<sup>7</sup> Carnegie Institution of Washington, Department of Terrestrial Magnetism, 5241 Broad Branch Road, Washington, DC 20015

<sup>8</sup> Steward Observatory, University of Arizona, 933 North Cherry Avenue, Tucson, AZ 85721

<sup>9</sup> Observatories of the Carnegie Institution of Washington, 813 Santa Barbara Street, Pasadena, CA 91101

<sup>10</sup> Lund Observatory, Box 43, SE-221 00 Lund, Sweden

<sup>11</sup> We prefer the neutral designation *intermediate luminosity optical transient* for this class of events since it does not impose a bias on the discovery method and initial mis-classification (as in the case of the “SN impostors” designation Van Dyk et al. 2000), it avoids various observational cuts on the optical properties (e.g., based on color as in the case of the “luminous red nova” designation Kulkarni et al. 2007) which may also be due to extrinsic effects (e.g., extinction), it is less cumbersome and more intuitive than designations based on prototype events (e.g., V838 Mon-like,  $\eta$  Car analogs), and perhaps most importantly, it makes no assumption about an eruptive versus explosive origin (as in the case of the “luminous red novae” or “SN impostors”).

pulse, nova eruption from an embedded common envelope white dwarf, or planet capture for V838 Mon (e.g., Retter et al. 2006 and references therein).

Regardless of the exact interpretation, it is clear that the various proposed eruption/explosion scenarios mark important phases in the evolution of massive stars, possibly on the path to diverse types of SNe. Therefore, a mapping between ILOTs and their progenitors will provide important constraints on the initial conditions (i.e., progenitors and circumstellar properties) of SN explosions. The present uncertainty in this mapping highlights the need for detailed observations that can uncover the conditions both prior to and during the ILOT events. These include the identification of progenitors, a detailed study of the circumstellar environment, and measurements of the event properties across the electromagnetic spectrum. Such observations will also allow us to determine the connection between the various proposed categories of ILOTs, and to map the overall diversity of this seemingly heterogeneous class.

In this paper we present such a combination of observations for an ILOT discovered in the nearby galaxy NGC 300 on 2008 April 24 UT (hereafter, NGC 300 OT2008-1). For the first time for such an event, we combine multi-wavelength observations (UV, optical, radio, and X-rays), high-resolution echelle spectroscopy, and archival *Hubble Space Telescope* and *Spitzer Space Telescope* data to show that NGC 300 OT2008-1 was the result of an eruption from a  $\sim 10\text{--}20 M_{\odot}$  dust-obscured and relatively compact star, possibly in a binary system. Our high-resolution spectra, the first for this event, resemble the yellow hypergiant star IRC+10420 (see also Bond et al. 2009), suggesting that NGC 300 OT2008-1 may mark a transition to a similar evolutionary stage. A comparison to the recent events SN 2008S and M85 OT2006-1 shows that all three events may have originated from the same phenomenon, but with a scatter in the energy release and circumstellar properties, that may point to a range of progenitor masses.

## 2. OBSERVATIONS

NGC 300 OT2008-1 was discovered by Monard (2008) on 2008 Apr 24.16 UT in the outskirts of the nearby galaxy NGC 300 ( $d = 1.9$  Mpc; Gieren et al. 2005) with an apparent brightness of 16.5 mag (unfiltered). Subsequent observations on May 14.14 UT revealed that the object had brightened to about 14.2 mag (Monard 2008). NGC 300 OT2008-1 was not detected in observations from 2008 Apr 17.1 UT, but only to a limit of 15.5 mag. It was also not detected in deeper observations taken on 2007 Dec 30.8 and 2008 Feb 8.75 UT to limiting magnitudes of 18.5 and 18.0 mag, respectively (Monard 2008). Since the transient was brightening at the discovery epoch, we adopt an event start time that is consistent with the most recent non-detection,  $t_0 \approx$  Apr 17 UT but note that the actual start time may have occurred earlier.

A low resolution spectrum of NGC 300 OT2008-1 obtained by Bond et al. (2008) on May 15.4 UT revealed emission lines corresponding to  $H\alpha$ ,  $H\beta$ , the Ca II IR triplet, and the [Ca II]  $\lambda\lambda 7293, 7325$  doublet (see also Bond et al. 2009). The marginally-resolved lines indicated velocities of  $\lesssim 800$  km  $s^{-1}$ , significantly lower than those of both classical novae and supernovae.

Following the announcement of the discovery and early spectroscopy, and given the unique opportunity to study a nearby ILOT in detail, we initiated observations across the electromagnetic spectrum, particularly high-resolution spec-

troscopy. In addition, we obtained archival *Hubble Space Telescope* and *Spitzer Space Telescope* observations at the position of the transient to search for a pre-discovery counterpart.

### 2.1. Astrometry

The original reported position of NGC 300 OT2008-1 was  $\alpha = 00^{\text{h}}54^{\text{m}}34.16^{\text{s}}$ ,  $\delta = -37^{\circ}38'28.6''$  (J2000), measured relative to the core of NGC 300 (Monard 2008). As part of our initial spectroscopic observations we obtained an  $r$ -band image of the field with the Low Dispersion Survey Spectrograph (LDSS-3) mounted on the Magellan/Clay 6.5-m telescope. Using 13 objects in common with the Naval Observatory Merged Astrometric Dataset (NOMAD), we measure the actual position of the transient to be  $\alpha = 00^{\text{h}}54^{\text{m}}34.52^{\text{s}}$ ,  $\delta = -37^{\circ}38'31.6''$  (J2000) with an uncertainty of about  $0.4''$  in each coordinate. This position is  $4.3''$  west and  $3.0''$  south of the IAUC position. The revised coordinates allowed us to search for a progenitor in archival HST observations, and led Thompson et al. (2008) to identify a counterpart in archival *Spitzer* observations (see §6).

### 2.2. Optical Spectroscopy

We obtained multiple low- and high-resolution optical spectra of NGC 300 OT2008-1 using LDSS-3 and the Magellan Inamori Kyocera Echelle (MIKE) spectrograph mounted on the Magellan/Clay 6.5-m telescope. A log of the observations, including the spectral coverage and resolution is provided in Table 1.

The LDSS-3 spectra were reduced using standard IRAF routines, while rectification and sky subtraction were performed using the method and software described in Kelson (2003). Wavelength calibration was performed using HeNeAr arc lamps, and air-to-vacuum and heliocentric corrections were applied. Flux calibration was performed using several spectrophotometric standard stars. The MIKE spectra were reduced using a custom reduction pipeline<sup>12</sup> written in Python. Wavelength calibration was performed using ThAr arc lamps, and air-to-vacuum and heliocentric corrections were applied.

### 2.3. Ground-based Optical Imaging

We obtained optical photometric observations with LDSS-3 in the *griz* filters on May 31.44 UT; see Table 3. The data were reduced using standard routines in IRAF. Photometry was performed relative to the standard star field E8-A. The resulting spectral energy distribution is shown in Figure 1.

### 2.4. Swift Ultraviolet and Optical Imaging

We obtained UV and optical observations with the *Swift* UV/optical telescope spanning from 2008 May 20 to October 15; see Table 2. The data were processed using standard routines within the HEASOFT package. Photometry of the transient in the UVW1 and *UBV* images was performed using the standard  $5''$  aperture; the source was not clearly detected in the UVW2 images. The light curves are shown in Figure 2, and the spectral energy distribution at the epoch of the LDSS-3 observations is shown in Figure 1.

### 2.5. X-rays

<sup>12</sup> <http://www.ociw.edu/Code/mike>

Simultaneous with the *Swift*/UVOT observations, data were also collected with the co-aligned X-ray Telescope for a total exposure time of 20.01 ks. No source is detected at the position of NGC 300 OT2008-1 to a  $3\sigma$  limit of  $F_X \lesssim 1.2 \times 10^{-14}$  erg s $^{-1}$  cm $^{-2}$ , where we have assumed a  $kT = 0.5$  keV thermal bremsstrahlung model and Galactic absorption,  $N_H = 3.1 \times 10^{20}$  cm $^{-2}$ . A power law model with a photon index of  $-2$  leads to a similar limit of  $\lesssim 1.6 \times 10^{-14}$  erg s $^{-1}$  cm $^{-2}$ . The corresponding limit on the luminosity is  $L_X \lesssim 5 \times 10^{36}$  erg s $^{-1}$ . This is lower by at least an order of magnitude than any X-ray detected supernova to date.

### 2.6. Radio

We observed NGC 300 OT2008-1 with the Very Large Array<sup>13</sup>) beginning on 2008 May 21.65 UT. No coincident radio source was detected to a limit of  $F_\nu \lesssim 90$   $\mu$ Jy ( $3\sigma$ ) at 8.46 GHz. Continued monitoring at frequencies between 4.86 and 22.5 GHz over the subsequent seven months revealed no radio emission, with the latest non-detection obtained on 2008 November 24 UT ( $F_\nu \lesssim 110$   $\mu$ Jy at 8.46 GHz). The upper limits imply a radio luminosity  $L_{\nu,\text{rad}} \lesssim 3 \times 10^{23}$  erg s $^{-1}$  Hz $^{-1}$ . This limit is at least two orders of magnitude below the least luminous radio SNe ever observed (type IIP SNe: Chevalier et al. 2006; type Ibc SN 2002ap Berger et al. 2002). It is also two orders of magnitude below the detected emission from the ‘‘SN impostor’’ SN 1961V (Stockdale et al. 2001).

### 3. BASIC PROPERTIES OF NGC 300 OT2008-1

The UV/optical spectral energy distribution (SED) on 2008 May 31 is shown in Figure 1. The data have been corrected for the low Galactic extinction,  $E(B-V) = 0.013$  mag (Schlegel et al. 1998). We find that the SED is well fit by a blackbody spectrum ( $\chi_r^2 = 7.6$  for 5 degrees of freedom) with a temperature of  $T = 4670 \pm 140$  K and a radius of  $R = (2.2 \pm 0.2) \times 10^{14}$  cm. The best-fit value of the host galaxy extinction is  $A_V = 0$  mag, with a  $1\sigma$  upper limit of  $A_V < 0.6$  mag. As we show below, the low intrinsic dust extinction is supported by our detection of weak interstellar Na I D absorption lines at the redshift of NGC 300, from which we infer negligible line of sight extinction,  $E(B-V) = 0.05 \pm 0.05$  mag.

Using an event start date of April 17 and assuming a constant expansion rate, the inferred velocity is about 600 km s $^{-1}$ , in good agreement with our measured velocity width of the H $\alpha$  emission line,  $\delta v \approx 640$  km s $^{-1}$  (see §4).

The optical/UV ‘‘bolometric’’ luminosity of NGC 300 OT2008-1 on May 31 is  $L_{\text{bol}} \approx 1.6 \times 10^{40}$  erg s $^{-1}$ , or  $M_{\text{bol}} \approx -11.8$  mag. This is about 4 magnitudes brighter than typical novae, and about 3–10 mag fainter than SNe (e.g., Kulkarni et al. 2007). The optical/UV emission fades slowly to  $\delta t \approx 65$  d with a decline rate of about 0.02 mag d $^{-1}$  (Figure 2). However, observations at  $\delta t \gtrsim 120$  d reveal significant steepening relative to the early decay rate, indicating a break in the light curves at  $\delta t \approx 80$ –100 d (detailed optical and near-IR light curves are presented in Bond et al. 2009). We return to this point in §8.

Using a roughly constant luminosity out to  $\approx 65$  d, we find that the total radiated energy is about  $10^{47}$  erg. Therefore, the outflow kinetic energy is at least as large, indicating an ejected mass of  $\gtrsim 0.03 M_\odot$ . The combination of low ejecta velocity and an intermediate luminosity suggest that

NGC 300 OT2008-1 is not a true SN explosion. Indeed, its luminosity is nearly an order of magnitude lower than even the claimed low-luminosity core-collapse SNe 1994N, 1997D, 1999br, 1999eu, and 2001dc, with  $L_{\text{bol}} \approx (5-10) \times 10^{40}$  erg s $^{-1}$  at  $t \lesssim 100$  d (Pastorello et al. 2004).

### 4. SPECTROSCOPIC PROPERTIES

The low-resolution spectra of NGC 300 OT2008-1 are shown in Figure 3. Convolution of the spectrum from May 31 with the transmission functions of the *griz* filters indicates that the flux calibration across the full spectral range is good to better than 10%. The most pronounced spectral features are the hydrogen Balmer emission lines, the [Ca II] doublet and the Ca II IR triplet in emission, and Ca II H&K in absorption. We additionally detect weak He I and Fe II emission lines, as well as O I and Na I in absorption. A full list of the lines detected at each epoch is provided in Table 4.

#### 4.1. Hydrogen Balmer Lines

The H $\alpha$  line is best fit by a Lorentzian profile with a velocity width (FWHM) of  $\delta v_{\text{FWHM}} \approx 640$  km s $^{-1}$ ; see Figure 4. The full width at continuum intensity (FWCI) is  $\delta v_{\text{FWCI}} \approx 3000$  km s $^{-1}$ . The width of the line indicates an expansion velocity of about 600 km s $^{-1}$ , in good agreement with our size and eruption date estimates (§3).

The H $\alpha$  flux remains relatively unchanged for the first 2 months, with  $F \approx 1.1 \times 10^{-13}$  erg s $^{-1}$  cm $^{-2}$ . The H $\beta$  line flux is  $1.9 \times 10^{-14}$  erg s $^{-1}$  cm $^{-2}$ , leading to  $F_{\text{H}\alpha}/F_{\text{H}\beta} \approx 6$ . This value is well in excess of  $F_{\text{H}\alpha}/F_{\text{H}\beta} \approx 3$  expected for case B recombination (at  $T = 5000$  K appropriate for the SED temperature of NGC 300 OT2008-1; §3). A large Balmer decrement may be due to dust extinction, but as we already showed above (and see also §5.1) the line of sight extinction to NGC 300 OT2008-1 is negligible. Instead, we conclude that the large Balmer decrement is due to interaction with a high density circumstellar environment, through a combination of Balmer self absorption and collisional excitation (Drake & Ulrich 1980). The observed ratio is indeed in good agreement with circumstellar interaction models (e.g., Chevalier & Fransson 1994).

Using the calculations of Drake & Ulrich (1980) for hydrogen emission at high electron densities, we find that the observed  $F_{\text{H}\alpha}/F_{\text{H}\beta}$  ratio requires a density of  $n_e \sim 10^{10} - 10^{12}$  cm $^{-3}$ . At this range of densities we expect the H $\gamma$  line to be suppressed to a minimum ratio of  $F_{\text{H}\gamma}/F_{\text{H}\beta} \approx 0.2$  (compared to 0.45 for case B recombination). Our non-detection of H $\gamma$  on May 31, with  $F_{\text{H}\gamma}/F_{\text{H}\beta} \lesssim 0.2$ , and the detection on June 22 with  $F_{\text{H}\gamma}/F_{\text{H}\beta} \approx 0.3$  support this conclusion. We note that the observed ratio  $F_{\text{H}\delta}/F_{\text{H}\beta} \approx 0.3$  (June 22) is somewhat higher than the expected value of about 0.1. We thus conclude that the Balmer lines arise from circumstellar interaction between the event ejecta and the pre-existing environment.

The H $\alpha$  luminosity resulting from circumstellar interaction is given by  $L_{\text{H}\alpha} \approx 1.1 \times 10^{38} n_{e,10}^2 R_{14}^3$  erg s $^{-1}$ , where we have assumed a shell with  $\delta R/R = 0.1$  and selected fiducial parameters for NGC 300 OT2008-1 as inferred above ( $n_e = 10^{10} n_{e,10}$  cm $^{-3}$  and  $R = 10^{14} R_{14}$  cm). Comparing with the observed H $\alpha$  luminosity of  $4 \times 10^{37}$  erg s $^{-1}$ , we find that  $n_e \sim 10^{10}$  cm $^{-3}$  and  $R \sim 10^{14}$ , in reasonable agreement with the values inferred from the Balmer line ratios and the blackbody fit to the SED. The shocked circumstellar material has an inferred mass of  $\sim 10^{-5} M_\odot$ . For a uniform wind with a constant velocity,  $v_w$ , this corresponds to a mass loss rate of  $\dot{M} \sim 10^{-3} v_{w,3} M_\odot$  yr $^{-1}$ , where  $v_w = 10^3 v_{w,3}$  km s $^{-1}$ . As a sanity check, we find

<sup>13</sup> The National Radio Astronomy Observatory is a facility of the National Science Foundation operated under cooperative agreement by Associated Universities, Inc.

that the inferred Thomson optical depth for these parameters is low,  $\tau_T \sim 0.1$ .

To summarize, the hydrogen Balmer emission line properties, coupled with the optical/UV spectral energy distribution, are indicative of an interaction between a low mass shell traveling at about  $600 \text{ km s}^{-1}$  with a high density circumstellar medium, resulting from a progenitor mass loss rate of  $\sim 10^{-3} M_{\odot} \text{ yr}^{-1}$ .

#### 4.2. Ca II Lines

We next turn to an investigation of the unusual Ca II permitted and forbidden lines, which are not generally detected in SN spectra (particularly at early time). As shown in Figure 4, the [Ca II] lines are significantly narrower than the  $H\alpha$  line, with  $\delta v_{\text{FWHM}} \approx 290 \text{ km s}^{-1}$ . Moreover, the lines are clearly asymmetric, ranging at continuum intensity from  $-200$  to  $+550 \text{ km s}^{-1}$ . We do not find any clear evolution in the line brightness and profile between May 23 and June 22 UT.

The Ca II IR triplet lines also exhibit a complex structure, with an overall symmetric profile, marked by strong absorption near the line center. The observed brighter blue wing indicates that the center of the absorption feature is redshifted relative to the emission center. We measure this shift to be about  $80 \text{ km s}^{-1}$ . The overall width of the lines is  $\delta v_{\text{FWHM}} \approx 560 \text{ km s}^{-1}$ , while the (unresolved) absorption component has  $\delta v_{\text{FWHM}} \approx 500 \text{ km s}^{-1}$ .

Finally, the Ca II H&K absorption lines exhibit an asymmetric profile with an extended red wing; see Figure 5. The overall velocity range at continuum intensity in the May 31 spectrum is  $-450$  to  $+900 \text{ km s}^{-1}$ . The lines appear to be somewhat narrower in the later spectrum from June 22. The large velocity width of the lines indicates that they are not interstellar in origin, but instead arise in the circumstellar environment. However, the fact that we observe in absorption gas that is both inflowing (red wing) and outflowing (blue wing), indicates that the lines do not arise exclusively from an outgoing wind associated with the eruption; in that case we would expect only the outflowing (blue) component to be observed in absorption.

The existence of material inflowing along the line of sight to NGC 300 OT2008-1 at velocities of up to  $900 \text{ km s}^{-1}$  can be explained as the result of: (i) gas infall from a previous eruption; or (ii) as the signature of wind outflow from a companion star impinging on the progenitor of NGC 300 OT2008-1. In the former scenario, the observed infall velocity, which we expect to be close to the progenitor's escape velocity, points to a massive and compact star such as a Wolf-Rayet star or a blue supergiant; the velocity is much larger than would be expected for a red giant, a red supergiant, or an asymptotic giant branch (AGB) progenitor as proposed by Thompson et al. (2008) and Bond et al. (2009). In the latter scenario, the companion would have to satisfy the same constraints (massive and compact) in order to launch a wind with  $\sim 10^3 \text{ km s}^{-1}$ . However, as we show in §6, the total progenitor system mass is in the range of  $\sim 10-20 M_{\odot}$ , making it difficult to accommodate an early-B or O star companion as required from the  $\sim 10^3 \text{ km s}^{-1}$  wind velocity (Lamers et al. 1995).

### 5. HIGH RESOLUTION SPECTROSCOPY

The general spectral properties outlined in the previous section are borne out in much greater detail and complexity in our high resolution spectra; see Figures 6–11. These are the first such observations available for NGC 300 OT2008-1. We further stress that neither M85 OT2006-1 nor SN 2008S, which

appear to share similar properties, have been observed at high spectral resolution so this is the first chance to investigate the properties of an ILOT in detail.

#### 5.1. Extinction from the Na I D Lines

Before we proceed with an analysis of the broad lines associated with the event itself, we use the Na I D absorption lines to determine the line of sight extinction within NGC 300. In the May 20 spectrum we detect unresolved lines with the expected 2:1 ratio of equivalent widths ( $0.17$  and  $0.08 \text{ \AA}$ ), indicating that they are optically thin; see Figure 12. We find no evidence for variation in the line profiles between the various epochs. From the narrowness and lack of variability we conclude that the lines are interstellar in origin. The measured equivalent widths correspond to a negligible line of sight extinction of  $E(B-V) = 0.05 \pm 0.05 \text{ mag}$  (Munari & Zwitter 1997). This inference is in good agreement with the lack of obvious extinction evidences in the optical/UV spectral energy distribution.

In the spectra between June 6 and July 2 we further detect broad Na I D absorption, with  $\delta v_{\text{FWHM}} \approx 300 \text{ km s}^{-1}$  (Figure 12). The lines are observed in emission in the spectrum from August 23 with a similar velocity width. The maximum absorption equivalent width is about  $0.5 \text{ \AA}$  in the July 2 spectrum, close to the saturation limit of the relation between extinction and Na I D equivalent width. The allowed range of  $E(B-V)$  for this value is  $\approx 0.2-0.5 \text{ mag}$ , in rough agreement with the upper limit of  $A_V < 0.6 \text{ mag}$  inferred from the SED of NGC 300 OT2008-1 (§3). We stress, however, that the relation between extinction and Na I D equivalent width is calibrated in the interstellar medium, and there is therefore no reason that it should equally hold in the complex circumstellar environment of NGC 300 OT2008-1, particularly in the presence of bright UV emission from the eruption itself. Indeed, as we show below, we find definitive evidence for dust destruction, which would undoubtedly alter the nature of the relation.

#### 5.2. Ca II H&K Lines

The broad and asymmetric Ca II H&K absorption lines are perhaps the most striking aspect of the spectrum (Figure 13). From the high resolution spectrum obtained on June 6 we find that the red wing of the lines is best modeled with a Lorentzian profile centered at  $+195 \text{ km s}^{-1}$  relative to the narrow component (the systemic velocity), and with a width of  $\delta v_{\text{FWHM}} \approx 700 \text{ km s}^{-1}$ ; a Gaussian profile with  $\delta v_{\text{FWHM}} \approx 860 \text{ km s}^{-1}$  provides a reasonable fit to the red wing as well. An extension of these profiles to the blue wing of the H&K lines significantly over-estimates the line absorption (Figure 13). The blue wing itself is well fit by a Lorentzian with a width of  $\delta v_{\text{FWHM}} = 200 \text{ km s}^{-1}$ .

It is unclear whether the two Ca II H&K absorption components (red and blue wings) arise in physically distinct regions (with the red side that corresponds to the blue component perhaps contributing to the red wing), or whether they arise from a kinematically asymmetric distribution of a single absorbing component. In the former case, we interpret the line profiles to arise from the presence of both outflowing and inflowing gas in the circumstellar environment due to distinct mass loss episodes, fragmentation of a previously ejected shell, or the presence of a binary companion wind. This scenario is similar to the model proposed by Humphreys et al. (2002) for the yellow supergiant star IRC+10420, in which recombined gas

no longer responds to radiation pressure, leading to infall at roughly the escape velocity. The measured infall velocity of  $\sim 10^3$  km s<sup>-1</sup> is significantly higher than  $\sim 10^2$  km s<sup>-1</sup> for absorption features in IRC+10420 Humphreys et al. (2002), indicating that the progenitor has a higher escape velocity (i.e., it is significantly more compact).

Subsequent echelle spectra reveal significant evolution in the Ca II H&K line profiles. First, the red absorption wing becomes progressively narrower with time, from about 700 km s<sup>-1</sup> on June 6 to about 270 km s<sup>-1</sup> on July 14. At the same time, the blue absorption wing becomes narrower and eventually starts to be overtaken by emission with a FWCI width of about 500 km s<sup>-1</sup> so that the overall line profile eventually resembles a reversed P Cygni profile. Both aspects of the line evolution can be explained as the result of recombination of Ca<sup>++</sup> gas produced through shocking of the initially absorbing gas by the eruption's outflowing material. In this scenario, the blue-shifted (outflowing) gas and the highest velocity inflowing gas are located physically closer to the progenitor, while the lower velocity infalling material will be eventually overtaken by the shock at a later time. A hint of this effect is seen in the low signal-to-noise spectrum from August 23, in which very little absorption in the red wing of the H&K lines is observed. The same process can also explain the shift from absorption to emission in the Na I D lines.

### 5.3. Ca II IR Triplet

The low-resolution spectra of NGC 300 OT2008-1 showed that the Ca II triplet emission lines are marked by broad absorption features offset to the red from the emission line center. At high resolution, the line profile is more complex, and the absorption is separated into multiple components; see Figure 14. In particular, in the June 6 spectrum there appear to be three distinct absorption components in addition to a narrow (interstellar) component, with velocity widths of 200, 100, and 40 km s<sup>-1</sup>. All three components are centered redward of the emission line peak, by 30, 200, and 80 km s<sup>-1</sup>, respectively. However, in our final spectrum from August 23, the line profiles become simpler, with just a single absorption component redshifted relative to the emission line center. This may again point to the presence of an initially complex circumstellar environment, which is partially overtaken and shocked by the outflowing ejecta.

The emission lines are symmetric and have a relatively constant width of  $\delta v_{\text{FWHM}} \approx 400$  km s<sup>-1</sup> in the various epochs. Since the ionCa2 IR lines are produced through radiative de-excitation from an excited state that is populated through absorption in the Ca II H&K lines, we expect the overall kinematic profiles of the H&K lines and the IR lines to match. However, the situation appears to be more complex here since the broad red absorption wing of the H&K lines does not appear to have a clear emission counterpart in the IR lines.

### 5.4. [Ca II] Lines

Another striking aspect of the echelle spectra is the strongly asymmetric profile of the [Ca II] lines, in which the blue wing is completely missing; see Figures 15 and 16. The red wing is best fit by a Lorentzian profile with a width of  $\delta v_{\text{FWHM}} \approx 170$  km s<sup>-1</sup> in the May 20 and June 6 spectra, decreasing to  $\delta v_{\text{FWHM}} \approx 140$  km s<sup>-1</sup> in the June 14 and July 2 spectra, and finally  $\delta v_{\text{FWHM}} \approx 75$  km s<sup>-1</sup> in the August 23 spectra. These lines are therefore significantly narrower than the Ca II IR lines and exhibit a more pronounced decrease in

width with time. This, along with the missing blue wing, indicate that the forbidden lines are produced in a physically distinct region from the IR lines. Indeed, to avoid collisional excitation and de-excitation out of the meta-stable excited state that is responsible for the [Ca II] emission, the lines need to be produced in a lower density environment compared to the IR lines and the hydrogen Balmer lines.

While the blue portion of the line is missing, we find no evidence for a P Cygni profile. Thus, the flux deficit is not due to absorption of the line emission by an optically thick outflow as generally observed for SNe. Instead, the line asymmetry may reflect an asymmetric distribution of the low density gas. In the context of the complex circumstellar environment inferred from the Ca II H&K and IR lines, it is likely that the red wing is produced in the low density outer layers of the inflowing gas, with the blue wing emission being absorbed by intervening material. This scenario also explains the lower velocity width compared to the H&K lines.

The spectra from July 2 and August 23 reveal the emergence of low level emission on the blue side of the forbidden lines. This increase coincides with the emergence of Ca II H&K emission on the blue side of the lines (§5.2), and it is likely due to the same process of Ca<sup>++</sup> recombination.

Finally, as discussed in Chevalier & Fransson (1994), we note that the energy required to ionize Ca<sup>+</sup> to Ca<sup>++</sup> from the meta-stable excited state (which if left undisturbed would produce the [Ca II] doublet through radiative de-excitation) corresponds to 1218.9 Å, or about 3.2 Å above the Ly $\alpha$  line. Thus, when the Ly $\alpha$  line is broader than about 800 km/s, the [Ca II] doublet emission can be strongly suppressed by ionization. For narrow Ly $\alpha$  emission this effect is inefficient and we expect stronger [Ca II] emission. This is indeed the case for NGC 300 OT2008-1, for which the typical lines widths are  $\lesssim 10^3$  km s<sup>-1</sup>. As a result, we expect that events like NGC 300 OT2008-1 will generally exhibit strong [Ca II] emission lines.

### 5.5. Hydrogen Balmer lines

The H $\alpha$  line, which appears to have a symmetric profile at low resolution, exhibits a more complex combination of emission and absorption when viewed at high spectral resolution; see Figure 17. At all epochs we find a narrow absorption feature close to the line center, with a width of  $\delta v_{\text{fwhm}} \approx 40$  km s<sup>-1</sup>. The absorption feature is redshifted by about 30 km s<sup>-1</sup> relative to the interstellar absorption of the Ca II lines. A second, but weaker, absorption component with a similar velocity width is detected at a velocity of  $-130$  km s<sup>-1</sup>.

The overall emission profile can be fit with either a Lorentzian profile or a combination of narrow and broad Gaussian profiles, which are slightly offset in velocity. The motivation behind the latter model is that the broad wings of the line appear to be somewhat asymmetric, with a slight deficit in the blue portion of the line. In the Lorentzian case, the line width remains relatively unchanged between May 20 and June 14 with  $\delta v_{\text{fwhm}} \approx 560$  km s<sup>-1</sup>, and decreases mildly to  $\delta v_{\text{fwhm}} \approx 440$  km s<sup>-1</sup> on July 2 and August 23. In the Gaussian model the narrow component appears to increase in width from about 295 km s<sup>-1</sup> on May 20 to about 400 km s<sup>-1</sup> in the spectra from June 6 to August 23. The broad component remains relatively unchanged with  $\delta v_{\text{fwhm}} \approx 1100$  km s<sup>-1</sup>. With only a mild change in width, and an increase in brightness relative to the continuum level, the H $\alpha$  equivalent width increases significantly with time, ranging from about 10 to 300

Å between May 20 and August 23.

The  $H\beta$  line exhibits the same profile as  $H\alpha$ ; see Figure 18. In the second epoch (which has a higher signal to noise ratio), the line is marked by a deep absorption feature with  $\delta v_{\text{fwhm}} \approx 70 \text{ km s}^{-1}$ , which is centered about  $80 \text{ km s}^{-1}$  redward of the emission line center. This component is thus wider than its counterpart  $H\alpha$  absorber, and it also exhibits a more pronounced shift relative to the line center. The  $H\beta$  line is again well fit by either a Lorentzian profile or a combination of narrow and wide Gaussians with offset line centers. In the former case, the line width remains unchanged with  $\delta v_{\text{fwhm}} = 380 \text{ km s}^{-1}$  until July 14, and decreases to about  $330 \text{ km s}^{-1}$  on August 23. In the Gaussian model, the line widths remain unchanged at  $350$  and  $1200 \text{ km s}^{-1}$ .

Finally, the  $H\gamma$  and  $H\delta$  lines exhibit similar profiles to  $H\alpha$  and  $H\beta$ . In particular, the  $H\gamma$  line exhibits blue-shifted weak absorption similar to that seen in  $H\alpha$ ; see Figures 19 and 20.

### 5.6. Additional Absorption and Emission Lines

In addition to the strong hydrogen Balmer lines and Ca II lines, we also detect the He I  $\lambda 5875$  emission line (Figure 12) and the O I triplets at  $7774$  and  $8446 \text{ Å}$  in absorption (Figure 21). In all cases the line widths are about  $300 \text{ km s}^{-1}$ . Moreover, the O I lines are clearly asymmetric with broad blue-shifted absorption extending to about  $300 \text{ km s}^{-1}$ . This is the opposite effect compared to the Ca II H&K lines, indicating that the absorption in these two species arises in distinct kinematic components.

In addition, we detect narrow absorption features of Ca II H&K, the Ca II IR triplet, and O I, with a typical width of  $\delta v_{\text{FWHM}} \approx 25 \text{ km s}^{-1}$ . It is unclear whether these narrow features are interstellar in origin, or are due to previous mass loss from the progenitor of NGC 300 OT2008-1, with a much lower wind velocity (possibly during a preceding red supergiant phase).

## 6. THE PROGENITOR OF NGC 300 OT2008-1

Our precise astrometry of NGC 300 OT2008-1 (§2.1) enabled a search for the progenitor in archival *Hubble Space Telescope* and *Spitzer Space Telescope* observations (see also Thompson et al. 2008; Bond et al. 2009).

### 6.1. Archival Hubble Space Telescope

The location of NGC 300 OT2008-1 was observed with the Advanced Camera for Surveys (ACS) on 2006 November 8 UT in the F475W (1488 s), F606W (1515 s), and F814W (1542 s) filters as part of program 10915 (PI: Delcanton). We retrieved the drizzled images from the HST archive and performed an astrometric tie relative to our initial LDSS-3 image (§2.1). The resulting astrometry has an rms of 30 mas in each coordinate.

We do not detect any objects at the position of NGC 300 OT2008-1 to the following  $5\sigma$  limits:  $m_{AB} > 28.1 \text{ mag}$  (F475W),  $m_{AB} > 27.8 \text{ mag}$  (F606W),  $m_{AB} > 27.3 \text{ mag}$  (F814W). The nearest object to the position of NGC 300 OT2008-1 is located about  $0.19''$  away, or about  $1.75 \text{ pc}$  at the distance of NGC 300. Images of the field at the location of NGC 300 OT2008-1 are shown in Figure 22.

### 6.2. Archival Spitzer Space Telescope

The location of NGC 300 OT2008-1 was observed with the Infra-Red Array Camera (IRAC) on 2007 December 28 UT, and with the Multiband Imaging Photometer for *Spitzer*

(MIPS) on 2007 July 6 and 16 UT. We retrieved the post-BCD data from the *Spitzer* archive and performed an astrometric tie relative to our initial LDSS-3 image (§2.1). The resulting astrometry has an rms of  $0.3''$  in each coordinate. Images of the field at the location of NGC 300 OT2008-1 are shown in Figures 23 and 24.

As noted by Prieto (2008) based on our reported astrometry of the transient Berger & Soderberg (2008), a coincident object is detected in the *Spitzer* data (see also Thompson et al. 2008). We performed photometry of this object using a 2-pixel aperture on the  $3.6$  and  $4.5 \mu\text{m}$  images, and a 3-pixel aperture on the  $5.8$ ,  $8.0$ , and  $24 \mu\text{m}$  images. The aperture size was selected to reduce contamination from nearby objects. We further used the standard zeropoints and aperture corrections provided in the *Spitzer* manual. The resulting spectral energy distribution of the coincident source, along with the HST upper limits, is shown in Figure 25.

### 6.3. Source Properties

A detailed discussion of the progenitor is presented by Thompson et al. (2008) who conclude that it is an extreme AGB star during a short-lived phase ( $\sim 10^4 \text{ yr}$ ) of its evolution. Below we provide an independent analysis of the *Spitzer* and HST observations. The spectral energy distribution is shown in Figure 25. We find that the SED is well fit by a blackbody profile ( $\chi_r^2 \approx 1.5$  for 3 degrees of freedom), indicating that the progenitor was enshrouded by dust prior to the eruption. The best-fit blackbody parameters are  $T = 340 \pm 10 \text{ K}$  and  $R = 330 \pm 20 \text{ AU}$ , with a resulting luminosity of  $5.7 \times 10^4 L_\odot$ . The total dust mass can be inferred by setting  $\tau = \kappa \rho R \approx 1$ , which for  $\kappa \approx 10 \text{ cm}^2 \text{ g}^{-1}$  (Prieto et al. 2008), corresponds to  $5 \times 10^{-3} M_\odot$ .

The fact that the progenitor was completely obscured by dust, while NGC 300 OT2008-1 exhibits negligible dust extinction ( $A_V < 0.6 \text{ mag}$ ; §3) demonstrates that the eruption destroyed the obscuring dust. Since the size of the dust-obscured region exceeds the shock radius of NGC 300 OT2008-1 by about a factor of 20 (§3), we conclude that the dust was destroyed through sublimation rather than shock heating. This process has been investigated by several authors, and we use here the formulation of Waxman & Draine (2000) developed in the context of gamma-ray bursts. The dust destruction radius is given by  $R_{\text{sub}} \approx 1.2 \times 10^{15} L_{40}^{1/2} \text{ cm}$ , for a typical grain size of  $0.1 \mu\text{m}$  and a dust absorption efficiency factor of order unity (Waxman & Draine 2000). For the radius of the dust-obscured region inferred above, we find that the luminosity required for sublimation is  $L \approx 2 \times 10^{41} \text{ erg s}^{-1}$ . This is about an order of magnitude larger than the bolometric luminosity measured for NGC 300 OT2008-1 on May 31 ( $\delta t \approx 45 \text{ d}$ ). The measured decay rate of about  $0.02 \text{ mag d}^{-1}$  extrapolated back to the estimated eruption date is not sufficient to overcome this discrepancy. We therefore conclude that either the early emission from NGC 300 OT2008-1 was characterized by a higher photospheric temperature, or the initial event produced a relatively bright UV flash with a luminosity of about  $2 \times 10^{41} \text{ erg s}^{-1}$ .

In either case, the destruction of the obscuring dust may be responsible for the strong Ca II emission, since the calcium is initially strongly depleted on dust grains.

## 7. INTERPRETATION: THE ERUPTION OF A MASSIVE STAR

Our detailed spectroscopic observations of NGC 300 OT2008-1, and the detection of its progenitor system in archival data, allow us to construct a basic model

of the event and its environment. The key observational results presented in the preceding sections are summarized as follows:

- The line of sight extinction is negligible as inferred from the UV/optical SED and the weak Na I D lines.
- Prior to the event, the progenitor system was enshrouded by dust, and had a luminosity of about  $6 \times 10^4 L_{\odot}$ , corresponding to a  $\sim 10 - 20 M_{\odot}$  star.
- The wide and asymmetric Ca II H&K absorption lines require gas infall at velocities of about  $10^3 \text{ km s}^{-1}$ , and hence a massive and relatively compact progenitor or companion.
- The Ca II IR lines and the hydrogen Balmer lines are symmetric and broad ( $\sim 300 - 600 \text{ km s}^{-1}$ ), and marked by narrow absorption redward of the emission line peak.
- The [Ca II] lines are extremely asymmetric, and significantly narrower than the other Ca II lines and hydrogen Balmer lines.
- None of the lines exhibit velocities in excess of  $\sim 10^3 \text{ km s}^{-1}$ , or P Cygni profiles.

These properties bear a striking resemblance to those of the massive yellow hypergiant IRC+10420 (e.g., de Jager 1998; Oudmaijer 1998; Humphreys et al. 2002; Smith et al. 2008; Bond et al. 2009), which is thought to be rapidly transitioning from a red supergiant phase to a luminous blue variable or Wolf-Rayet phase. Like the progenitor of NGC 300 OT2008-1, IRC+10420 is marked by a bright infrared excess resulting from a dusty nebula, but unlike NGC 300 OT2008-1 the central object is not completely obscured. The luminosity of IRC+10420,  $\approx 5 \times 10^5 L_{\odot}$ , is about an order of magnitude larger than our inferred luminosity of the progenitor of NGC 300 OT2008-1 (§3). This points either to a lower mass or a somewhat earlier evolutionary stage for the progenitor of NGC 300 OT2008-1. Equally important, IRC+10420 exhibits essentially identical hydrogen Balmer and Ca II IR line profiles to those seen in our high resolution spectra, including the redshifted narrow absorption feature (see Figures 4 and 5 of Humphreys et al. 2002 and Figures 3 and 4 of Oudmaijer 1998).

At the same time, there are some distinct difference between the spectroscopic properties of NGC 300 OT2008-1 and IRC+10420. First, the ionCa2 H&K lines in IRC+10420 are symmetric and significantly narrower than those observed in NGC 300 OT2008-1 (Oudmaijer 1998). Second, the [Ca II] emission lines in IRC+10420 appear to be symmetric (Oudmaijer 1998; Humphreys et al. 2002), although like in the case of NGC 300 OT2008-1 they are significantly narrower than the hydrogen Balmer lines and the Ca II IR lines. Third, the Ca II IR lines, which extend to about  $\pm 100 \text{ km s}^{-1}$  (Humphreys et al. 2002), are significantly narrower than in NGC 300 OT2008-1. Finally, while the  $H\alpha$  profiles in both objects are generally similar, the red and blue emission peaks of IRC+10420 have a similar width to the central absorption (Humphreys et al. 2002), whereas in the case of NGC 300 OT2008-1 the emission peaks are significantly wider. In both cases the  $H\alpha$  line exhibit a broad wing, which is interpreted as the effect of electron scattering in the case

of IRC+10420 (Humphreys et al. 2002). In the spectrum of NGC 300 OT2008-1, however, the core of the line is broader and the wings are less pronounced, and we interpret the profile as due to circumstellar interaction of an outflow with a velocity of about  $600 \text{ km s}^{-1}$  (as opposed to a outflowing wind velocity of only  $50 \text{ km s}^{-1}$  inferred for IRC+10420).

The combination of these various properties suggests that in broad terms the progenitor of NGC 300 OT2008-1 may be similar to IRC+10420, but it may have been in a somewhat different evolutionary stage prior to the eruption, with still complete dust obscuration. In addition, the eruption itself appears to have produced a significantly faster, more energetic, and more luminous outflow compared to the “quiescent” state of IRC+10420. Thus, it is possible that NGC 300 OT2008-1 marks the initial transition to an IRC+10420-like object, and that as the eruption fades, its properties will converge to those of IRC+10420.

## 8. COMPARISON WITH M85 OT2006-1 AND SN 2008S

We finally turn to a comparison of NGC 300 OT2008-1 with two recent events that exhibit several similar properties: M85 OT2006-1 and SN 2008S. SN 2008S was discovered on February 1.8 UT in NGC 6946 ( $d \approx 5.6 \text{ Mpc}$ ) and had an absolute magnitude of  $M_V \approx -14 \text{ mag}$  (taking into account significant Galactic and host obscuration of  $A_V \approx 2.5 \text{ mag}$ ; Prieto et al. 2008; Smith et al. 2008). The *R*-band light curve of SN 2008S from Smith et al. (2008) is shown in Figure 2. The temporal evolution is remarkably similar to that of NGC 300 OT2008-1, namely a relatively stable decay rate of about  $0.035 \text{ mag d}^{-1}$  from about 30 to 100 days. However, unlike NGC 300 OT2008-1, the optical emission from SN 2008S does not exhibit a clear steepening at later times, and it may indeed flatten to a decay rate of about  $0.01 \text{ mag d}^{-1}$  from 130 to 270 days.

In Figure 26 we present a low-resolution spectrum of SN 2008S that we obtained on 2008 Mar 15.5 UT ( $\delta t \approx 42 \text{ d}$ ) using the ARC 3.5-m telescope at Apache Point Observatory. The resolution of the spectrum is  $6.5 \text{ \AA}$ , or about  $300 \text{ km s}^{-1}$ . Neglecting extinction, we find that the overall continuum shape and brightness are characterized by a blackbody profile with  $T \approx 4800 \text{ K}$  and  $R \approx 1.6 \times 10^{14} \text{ cm}$ , similar to the properties inferred for NGC 300 OT2008-1 at a similar epoch of about 44 d (Figure 25). The inferred bolometric absolute magnitude is  $\approx -11.3 \text{ mag}$ . However, if we include the estimated extinction of  $A_V \approx 2.5 \text{ mag}$ , we find that the spectrum requires a higher temperature,  $T \approx 10^4 \text{ K}$ , and a smaller radius,  $R \approx 9 \times 10^{13} \text{ cm}$ , leading to an overall absolute magnitude of  $M_{\text{bol}} \approx -13.9 \text{ mag}$ , similar to the values inferred by Smith et al. (2008) from similar spectroscopic observations. Thus, SN 2008S has a bolometric luminosity that is nearly an order of magnitude larger than NGC 300 OT2008-1. Combined with the similar temporal evolution, we conclude that SN 2008S released about an order of magnitude more energy than NGC 300 OT2008-1,  $E \sim 10^{48} \text{ erg}$  (see also Smith et al. 2008).

The overall similarity is also evident in the dominant spectral features of both events. SN 2008S exhibits strong and narrow hydrogen Balmer lines, [Ca II] lines, and Ca II IR lines. The  $H\alpha$  line is resolved with a width of  $\delta v_{\text{fwhm}} \approx 1200 \text{ km s}^{-1}$ , about a factor of 2 times broader than for NGC 300 OT2008-1. As in the case of NGC 300 OT2008-1, the Ca II IR triplet lines exhibit a similar width to that of  $H\alpha$ ,  $\delta v_{\text{fwhm}} \approx 1300 \text{ km s}^{-1}$ . The [Ca II] lines are only marginally resolved, with  $\delta v_{\text{fwhm}} \approx 350 \text{ km s}^{-1}$ . This is again a factor of 2 times broader

than in NGC 300 OT2008-1, and comparably narrower than the H $\alpha$  line. Due to the low resolution of the spectrum it is unclear whether the [Ca II] lines are asymmetric. Unlike in the case of NGC 300 OT2008-1, we do not detect Ca II H&K absorption or He I emission.

Finally, perhaps the most important similarity between SN 2008S and NGC 300 OT2008-1 is the detection of a coincident *Spitzer* source in both events (Prieto et al. 2008; Thompson et al. 2008). As shown in Figure 25, the SEDs of both coincident sources are similar, with  $T \approx 440$  K,  $R \approx 160$  AU, and  $L \approx 4 \times 10^4 L_{\odot}$  for SN 2008S. Thus, both events appear to arise from objects of a similar luminosity and in a similar evolutionary stage. Thompson et al. (2008) recently argued that the progenitors of both events are extreme AGB stars with masses of  $\sim 10 M_{\odot}$ , and that the events themselves are likely electron-capture SNe. Smith et al. (2008), on the other hand, advocated a scenario for SN 2008S of a super-Eddington eruption that results in significant mass loss. They further note an overall similarity to IRC+10420, and speculate that SN 2008S resembles an eruption of a  $\sim 20 M_{\odot}$  blue supergiant, rather than a lower mass red supergiant as advocated by Thompson et al. (2008). Our high resolution spectroscopic observations of NGC 300 OT2008-1, and their close resemblance to the spectrum of IRC+10420, support the interpretation of Smith et al. (2008). Still, while both events appear to arise from similar objects, these progenitors are clearly capable of producing eruptions with an energy release that spans at least an order of magnitude.

We next turn to a comparison with M85 OT2006-1. As shown in Figure 1, the spectral energy distribution of this event closely resembles NGC 300 OT2008-1, with a nearly identical bolometric luminosity of about  $-12$  mag (Kulkarni et al. 2007). The light curve evolution is also similar (Figure 2), with a comparable decay rate during the first  $\sim 70$  days, followed by a significant steepening at later time. Thus, M85 OT2006-1 appears to be a clear analog of both NGC 300 OT2008-1 and SN 2008S.

Unfortunately, the low-resolution spectra of M85 OT2006-1, obtained about 1 and 48 d after discovery (Kulkarni et al. 2007), had a low signal-to-noise ratio that precludes a detailed analysis. Still, the second spectrum does exhibit a narrow H $\alpha$  emission line with  $\delta v_{\text{fwhm}} \approx 350$  km s $^{-1}$ , about two times narrower than in NGC 300 OT2008-1. Additional weak features possibly corresponding to Ca II H&K and Fe II  $\lambda 6544$  may also be discerned in the spectrum (see Figure 3 of Kulkarni et al. 2007). These possible features provide additional support for a common origin with NGC 300 OT2008-1.

On the other hand, the environments of NGC 300 OT2008-1 and M85 OT2006-1 differ significantly. In the case of M85 OT2006-1, the host is an early type galaxy (with a mean age of  $\sim 1.6$  Gyr), and the environment of the transient itself contains no stars brighter than  $M_z \approx -6.2$  mag, corresponding to a mass of  $\lesssim 7 M_{\odot}$  (Ofek et al. 2008). The local environment of NGC 300 OT2008-1, on the other hand, contains stars with inferred masses of  $\sim 14 M_{\odot}$  (Bond et al. 2009), in line with the inferred mass of the progenitor system. Thus, it appears that different channels/progenitors may lead to the formation of similar transient outbursts.

Given the overall similarity between the three events it is reasonable to conclude that they share a common origin. Thanks to our detailed high-resolution spectroscopic observations of NGC 300 OT2008-1, an intimate connection with objects like IRC+10420 appears likely (in agreement with previous speculation Smith et al. 2008) but may not be required

(e.g., M85 OT2006-1). From the overall similarity we further conclude that none of the three transients are likely to have resulted from the explosion of the progenitor star. Instead, the eruptions may mark a shift in the evolutionary stage from complete obscuration to a yellow supergiant phase, and eventually a Wolf-Rayet star. Clearly, such a transition apparently leads to overall common features, but in detail the energy and velocity of the outflow appear to vary by at least an order of magnitude.

## 9. SUMMARY AND CONCLUSIONS

We presented the first high-resolution spectroscopic observations for the intermediate luminosity optical transient NGC 300 OT2008-1, as well as multi-wavelength observations (UV/optical/radio/X-ray) and an independent analysis of archival *Spitzer* and HST observations of its progenitor (see also Thompson et al. 2008; Bond et al. 2009). The preponderance of photometric and spectroscopic evidence indicate that this event is not a supernova, but is instead the result of an eruption on a  $\sim 10 - 20 M_{\odot}$  blue supergiant or pre-Wolf-Rayet star, possibly in a binary system. The high-resolution spectra reveal the presence of a complex circumstellar environment, marked by outflows and possible inflow from previous ejections or from a companion wind. The observed inflow velocities are indicative of a massive and relatively compact progenitor, not a highly extended red supergiant, in contrast to the interpretation of Thompson et al. (2008) and Bond et al. (2009). Alternatively, the progenitor may be part of a binary system in which the companion wind (with a velocity of  $\sim 10^3$  km s $^{-1}$ ) is observed in absorption along the line of sight. In this scenario, however, it may be difficult to accommodate the relatively low total system mass of  $\lesssim 20 M_{\odot}$ .

The outburst itself gave rise to an outflow with a velocity of  $\sim 600$  km s $^{-1}$  and a kinetic energy of at least  $10^{47}$  erg. No radio or X-ray emission are detected to limits that are significantly dimmer than the faintest SNe detected to date, indicating a lack of fast ejecta (with  $v \gtrsim 0.1c$ ).

NGC 300 OT2008-1 closely resembles two previous events, M85 OT2006-1 and SN 2008S, in terms of its intermediate luminosity and spectral properties. It also shares with SN 2008S a dust-obscured progenitor with a luminosity of a  $\sim 10^5 L_{\odot}$ . Our detailed comparison reveals that the outburst and progenitor properties point to a common origin, but with a range of outburst energy and velocity of nearly an order of magnitude. We also note a resemblance between the spectroscopic properties of NGC 300 OT2008-1 and those of the luminous yellow supergiant IRC+10420. However, the latter is about an order of magnitude more luminous than the progenitor of NGC 300 OT2008-1, and its observed “quiescent” outflow has a velocity of only  $\sim 50$  km s $^{-1}$ . These differences raise the possibility that NGC 300 OT2008-1 marks the transition to an IRC+10420-like state, or that its progenitor is simply a lower mass analogue.

While our optical/UV photometry and low-resolution spectroscopy are of similar quality to those of SN 2008S and M85 OT2006-1, our extensive echelle spectroscopy provides a much deeper view of the circumstellar environment than previously available for this class of events. Indeed, we stress that the overall photometric behavior and general spectroscopic features observed in NGC 300 OT2008-1 may be generic to a broad class of stellar eruptions with an intermediate velocity in the presence of a dense circumstellar environment. For example, the 2002 eruption of V838 Mon was similar in broad terms to that of NGC 300 OT2008-1,

M85 OT2006-1, and SN 2008S, based on a comparable light curve behavior and spectroscopic evidence for narrow H $\alpha$  and Ca II lines (e.g., Rushton et al. 2005). However, the eruption was about an order of magnitude less luminous than NGC 300 OT2008-1 and M85 OT2006-1, and the progenitor appears to have been a lower mass star. We conclude that a clear understanding of the broad range of ILOTs requires high-resolution spectroscopy to assess the detailed properties of the circumstellar environment, as well as the identification of progenitors; optical/IR photometry and low-resolution spectroscopy alone are not likely to be sufficient.

Finally, the main prediction of our model is that the progenitor of NGC 300 OT2008-1 should be visible following the decay of the event. If the current eruption is similar to previous events that produced the now-destroyed dust shell, than the progenitor would again be visible as an obscured IR source. However, if only a minor amount of dust reforms, we predict that the spectrum will more closely resemble that of IRC+10420. In either case it appears that events like NGC 300 OT2008-1 represent an important stage in the

evolution of massive stars toward their eventual demise in SN explosions. The advent of facilities such as Pan-STARRS and LSST will lead to an increased rate of detections of events similar to NGC 300 OT2008-1. From the observations presented here it is clear that multi-wavelength follow-up, in particular high-resolution spectroscopy, which is not typically attempted for SNe (cf. SN 2008S), is critical for a detailed understanding of the eruption process and the properties of the progenitor(s).

This paper includes data gathered with the 6.5 meter Magellan Telescopes located at Las Campanas Observatory, Chile. We thank David Sand for obtaining the LDSS-3 spectrum on 2008 June 5, Bruce Draine for insightful discussions about the spectral properties of NGC 300 OT2008-1, and Ranga Chary for assistance with the *Spitzer* data. AMS acknowledges support by NASA through a Hubble Fellowship grant. RAC acknowledges support from an NSF grant AST-0807727.

#### REFERENCES

- Berger, E., Kulkarni, S. R., & Chevalier, R. A. 2002, *ApJ*, 577, L5  
 Berger, E., & Soderberg, A. 2008, *The Astronomer's Telegram*, 1544, 1  
 Bond, H. E., Bonanos, A. Z., Humphreys, R. M., Berto Monard, L. A. G., Prieto, J. L., & Walter, F. M. 2009, *ArXiv e-prints*  
 Bond, H. E., Walter, F. M., & Velasquez, J. 2008, *IAU Circ.*, 8946, 2  
 Chevalier, R. A., & Fransson, C. 1994, *ApJ*, 420, 268  
 Chevalier, R. A., Fransson, C., & Nymark, T. K. 2006, *ApJ*, 641, 1029  
 de Jager, C. 1998, *A&A Rev.*, 8, 145  
 Drake, S. A., & Ulrich, R. K. 1980, *ApJS*, 42, 351  
 Gieren, W., Pietrzyński, G., Soszyński, I., Bresolin, F., Kudritzki, R.-P., Minniti, D., & Storm, J. 2005, *ApJ*, 628, 695  
 Goodrich, R. W., Stringfellow, G. S., Penrod, G. D., & Filippenko, A. V. 1989, *ApJ*, 342, 908  
 Humphreys, R. M., Davidson, K., & Smith, N. 2002, *AJ*, 124, 1026  
 Kelson, D. D. 2003, *PASP*, 115, 688  
 Kulkarni, S. R., et al. 2007, *Nature*, 447, 458  
 Lamers, H. J. G. L. M., Snow, T. P., & Lindholm, D. M. 1995, *ApJ*, 455, 269  
 Monard, L. A. G. 2008, *IAU Circ.*, 8946, 1  
 Munari, U., et al. 2002, *A&A*, 389, L51  
 Munari, U., & Zwitter, T. 1997, *A&A*, 318, 269  
 Ofek, E. O., et al. 2008, *ApJ*, 674, 447  
 Oudmaijer, R. D. 1998, *A&AS*, 129, 541  
 Pastorello, A., et al. 2007, *Nature*, 449, 1  
 Pastorello, A., et al. 2004, *MNRAS*, 347, 74  
 Prieto, J. L. 2008, *The Astronomer's Telegram*, 1550, 1  
 Prieto, J. L., et al. 2008, *ApJ*, 681, L9  
 Retter, A., Zhang, B., Siess, L., & Levinson, A. 2006, *MNRAS*, 370, 1573  
 Rushton, M. T., et al. 2005, *MNRAS*, 360, 1281  
 Schlegel, D. J., Finkbeiner, D. P., & Davis, M. 1998, *ApJ*, 500, 525  
 Smith, N., Ganeshalingam, M., Li, W., Chornock, R., Steele, T. N., Silverman, J. M., Filippenko, A. V., & Mobberley, M. P. 2008, *ArXiv e-prints*  
 Soker, N., & Tylenda, R. 2006, *MNRAS*, 373, 733  
 Stockdale, C. J., Rupen, M. P., Cowan, J. J., Chu, Y.-H., & Jones, S. S. 2001, *AJ*, 122, 283  
 Thompson, T. A., Prieto, J. L., Stanek, K. Z., Kistler, M. D., Beacom, J. F., & Kochanek, C. S. 2008, *ArXiv e-prints*  
 Van Dyk, S. D., Filippenko, A. V., Chornock, R., Li, W., & Challis, P. M. 2005, *PASP*, 117, 553  
 Van Dyk, S. D., Peng, C. Y., King, J. Y., Filippenko, A. V., Treffers, R. R., Li, W., & Richmond, M. W. 2000, *PASP*, 112, 1532  
 Waxman, E., & Draine, B. T. 2000, *ApJ*, 537, 796

TABLE 1  
SPECTROSCOPIC OBSERVATIONS

UT Date	Instrument	Exposure (s)	Grism	Slit	Wavelength (Å)	Resolution (Å)
2008 May 20.42	MIKE	2 × 600	Blue	0.7''	3400–5100	0.10
	MIKE	2 × 600	Red	0.7''	4900–9400	0.21
2008 May 23.43	LDSS-3	1 × 900	VPH-red	1''	6000–9700	6.2
2008 May 31.40	LDSS-3	2 × 600	VPH-blue	1''	3800–6500	3.4
	LDSS-3	2 × 720	VPH-red	1''	6000–9700	6.2
2008 June 5.41	LDSS-3	1 × 900	VPH-red	1''	6000–9700	6.2
2008 June 6.40	MIKE	3 × 600	Blue	1''	3400–5100	0.13
	MIKE	3 × 600	Red	1''	4900–9400	0.28
2008 June 14.40	MIKE	2 × 1200	Blue	0.7''	3400–5100	0.10
	MIKE	2 × 1200	Red	0.7''	4900–9400	0.21
2008 June 22.42	LDSS-3	1 × 900	VPH-blue	1''	3850–6600	3.4
	LDSS-3	1 × 900	VPH-red	1''	6050–9750	6.2
2008 July 2.35	MIKE	2 × 900	Blue	1''	3400–5100	0.13
	MIKE	2 × 900	Red	1''	4900–9400	0.28
2008 July 14.36	MIKE	2 × 900	Blue	1''	3400–5100	0.13
	MIKE	2 × 900	Red	1''	4900–9400	0.28
2008 August 23.32	MIKE	2 × 900	Blue	0.7''	3400–5100	0.10
	MIKE	2 × 900	Red	0.7''	4900–9400	0.21

NOTE. — Journal of spectroscopic observations of the transient in NGC 300.

TABLE 2  
*Swift* UV/OPTICAL TELESCOPE OBSERVATIONS

UT Date	Filter	Exposure (s)	Magnitude	Flux Density ( $10^{-15}$ erg s $^{-1}$ cm $^{-2}$ Å $^{-1}$ )
2008 May 20.01	UVW2	5723	18.24 ± 0.03	0.27 ± 0.01
2008 May 25.03	UVW1	3877	17.67 ± 0.03	0.34 ± 0.01
2008 May 25.04	U	1551	16.13 ± 0.01	1.25 ± 0.01
2008 May 25.04	B	773	15.68 ± 0.01	3.46 ± 0.03
2008 May 25.04	V	691	14.88 ± 0.02	4.18 ± 0.06
2008 June 4.68	UVW1	1295	17.90 ± 0.05	0.27 ± 0.01
2008 June 4.67	U	1599	16.43 ± 0.01	0.94 ± 0.01
2008 June 4.68	B	1856	15.93 ± 0.01	2.75 ± 0.02
2008 June 4.67	V	2006	15.02 ± 0.02	3.69 ± 0.05
2008 June 19.39	UVW1	1765	17.96 ± 0.05	0.26 ± 0.01
2008 June 19.39	U	879	16.70 ± 0.02	0.74 ± 0.01
2008 June 19.39	B	879	16.22 ± 0.02	2.11 ± 0.03
2008 June 19.39	V	879	15.21 ± 0.02	3.08 ± 0.05
2008 August 14.17	UVW1	746	> 20.6	< 0.02
2008 August 14.17	U	428	18.57 ± 0.12	0.13 ± 0.02
2008 August 14.17	B	428	18.44 ± 0.08	0.27 ± 0.02
2008 August 14.17	V	428	17.73 ± 0.08	0.30 ± 0.02
2008 August 15.04	UVW1	727	> 20.7	< 0.02
2008 August 15.04	U	467	18.65 ± 0.13	0.12 ± 0.01
2008 August 15.04	B	467	18.59 ± 0.09	0.24 ± 0.02
2008 August 15.04	V	467	17.65 ± 0.08	0.33 ± 0.02
2008 August 26.60	UVW1	1522	> 21.4	< 0.01
2008 August 26.60	U	1024	19.99 ± 0.15	0.036 ± 0.005
2008 August 26.60	B	1024	19.16 ± 0.13	0.14 ± 0.01
2008 August 26.59	V	1024	18.60 ± 0.10	0.14 ± 0.01
2008 October 15.02	U	716	> 21.2	< 0.01
2008 October 15.02	B	646	> 21.2	< 0.02
2008 October 15.01	V	716	> 19.8	< 0.04

NOTE. — Journal of *Swift* UV/Optical Telescope observations of NGC 300 OT2008-1. Central wavelengths for the various filters are: 1880 Å (UVW2), 2510 Å (UVW1), 3450 Å (U), 4390 Å (B), and 5440 Å (V).

TABLE 3  
OPTICAL PHOTOMETRIC OBSERVATIONS

UT Date	Telescope	Filter	Exposure (s)	Magnitude
2008 May 31.44	Magellan	g	5	$15.29 \pm 0.04$
2008 May 31.40	Magellan	r	10	$14.59 \pm 0.04$
2008 May 31.44	Magellan	i	5	$14.28 \pm 0.04$
2008 May 31.44	Magellan	z	10	$14.06 \pm 0.04$

NOTE. — Journal of optical observations of NGC 300 OT2008-1 from May 31.4 UT.

TABLE 4  
LINE IDENTIFICATION IN THE LOW-RESOLUTION SPECTRA

Line	Date	Wavelength (Å)	Velocity (km s <sup>-1</sup> )	EW (Å)	FWHM (Å)	Flux (erg cm <sup>-2</sup> s <sup>-1</sup> )
Ca II H	May 31	3938.84	310	10.5	12.1	...
	June 22	3938.30	270	7.5	8.7	...
Ca II K	May 31	3973.78	315	7.9	9.3	...
	June 22	3973.47	295	5.5	7.0	...
Hδ	May 31	4102.51	-30	-4.7	14.1	$9.8 \times 10^{-15}$
	June 22	4104.32	105	-5.7	6.7	$7.0 \times 10^{-15}$
Hγ	June 22	4343.25	110	-5.6	7.2	$8.6 \times 10^{-15}$
Hβ	May 31	4864.35	100	-3.9	9.0	$1.3 \times 10^{-14}$
	June 22	4864.28	100	-11.2	6.7	$2.5 \times 10^{-14}$
?	May 31	5857.10	...	0.2	7.2	...
	June 22	5856.00	...	0.6	7.9	...
He I 5877.25	May 31	5878.96	90	-1.0	9.8	$3.9 \times 10^{-15}$
	June 22	5880.13	145	-2.6	7.6	$7.3 \times 10^{-15}$
Na I D	May 31	5895.65	55	1.0	10.0	...
	June 22	5894.75	10	2.1	10.2	...
Fe II 5993.03	May 31	5999.51	325	-0.5	9.9	$2.1 \times 10^{-15}$
	June 22	5998.22	260	-0.7	7.1	$2.0 \times 10^{-15}$
Fe II 6434.46	May 23	6437.31	130	-0.7	21.3	$3.7 \times 10^{-15}$
	May 31	6434.78	15	-0.8	20.7	$3.1 \times 10^{-15}$
	June 5	6436.56	100	-0.9	18.5	$3.2 \times 10^{-15}$
	June 22	6438.13	170	-1.0	9.0	$3.1 \times 10^{-15}$
Fe II 6517.85	May 23	6523.81	270	-0.3	7.3	$1.4 \times 10^{-15}$
	May 31	6522.95	235	-0.6	9.6	$2.1 \times 10^{-15}$
	June 5	6522.66	220	-0.5	7.5	$1.9 \times 10^{-15}$
	June 22	6521.58	170	-1.4	8.0	$4.3 \times 10^{-15}$
Hα	May 23	6569.94	240	-20.2	16.2	$1.0 \times 10^{-13}$
	May 31	6568.86	190	-23.2	15.3	$9.2 \times 10^{-14}$
	June 5	6568.74	190	-27.4	14.9	$9.3 \times 10^{-14}$
	June 22	6468.02	155	-46.0	13.3	$1.5 \times 10^{-13}$
He I 6679.99	May 23	6684.60	210	-0.7	17.5	$3.2 \times 10^{-15}$
	May 31	6684.99	225	-0.8	13.0	$3.0 \times 10^{-15}$
	June 5	6684.64	210	-0.7	8.9	$2.5 \times 10^{-15}$
	June 22	6684.46	200	-1.6	11.5	$5.1 \times 10^{-15}$
He I 7067.14	May 23	7068.33	50	-0.2	6.4	$8.3 \times 10^{-16}$
	May 31	7068.51	60	-0.3	5.4	$9.4 \times 10^{-16}$
	June 5	7069.89	120	-0.4	6.6	$1.4 \times 10^{-15}$
	June 22	7071.10	170	-0.7	10.7	$2.1 \times 10^{-15}$
[CaII] 7293.48	May 23	7299.60	250	-4.7	4.3	$2.0 \times 10^{-14}$
	May 31	7299.20	235	-5.2	5.5	$1.8 \times 10^{-14}$
	June 5	7299.45	245	-3.6	4.0	$1.1 \times 10^{-14}$
	June 22	7298.22	195	-5.4	5.2	$1.6 \times 10^{-14}$
[CaII] 7325.91	May 23	7332.04	250	-4.5	5.4	$1.9 \times 10^{-14}$
	May 31	7331.62	235	-4.6	6.5	$1.6 \times 10^{-14}$
	June 5	7331.80	240	-3.7	5.2	$1.1 \times 10^{-14}$
	June 22	7330.61	195	-4.8	6.1	$1.4 \times 10^{-14}$
Fe II 7464.44	May 23	7468.98	180	-0.8	24.5	$3.4 \times 10^{-15}$
	May 31	7468.14	150	-0.7	16.0	$2.4 \times 10^{-15}$
	June 5	7467.85	135	-1.0	20.1	$3.0 \times 10^{-15}$
	June 22	7467.54	125	-1.4	19.2	$4.0 \times 10^{-15}$
Fe II 7713.83	May 23	7723.98	395	-1.0	24.2	$4.0 \times 10^{-15}$
	May 31	7720.87	275	-0.7	13.8	$2.5 \times 10^{-15}$
	June 5	7721.19	285	-0.7	11.6	$2.1 \times 10^{-15}$
	June 22	7720.93	275	-1.1	11.1	$3.1 \times 10^{-15}$
O I 7774.08 <sup>a</sup>	May 23	7780.29	240	1.4	8.9	...
	May 31	7778.85	185	1.9	10.6	...
	June 5	7778.87	185	1.9	10.3	...
	June 22	7776.96	110	2.0	9.4	...
O I 8448.57 <sup>b</sup>	May 23	8454.78	220	0.5	4.9	...
	May 31	8452.95	155	0.4	5.6	...
	June 5	8452.76	150	0.4	5.8	...
	June 22	7776.96	110	2.0	9.4	...

NOTE. — Emission and absorption features identified in the low resolution spectra of NGC300-2008-OT1.

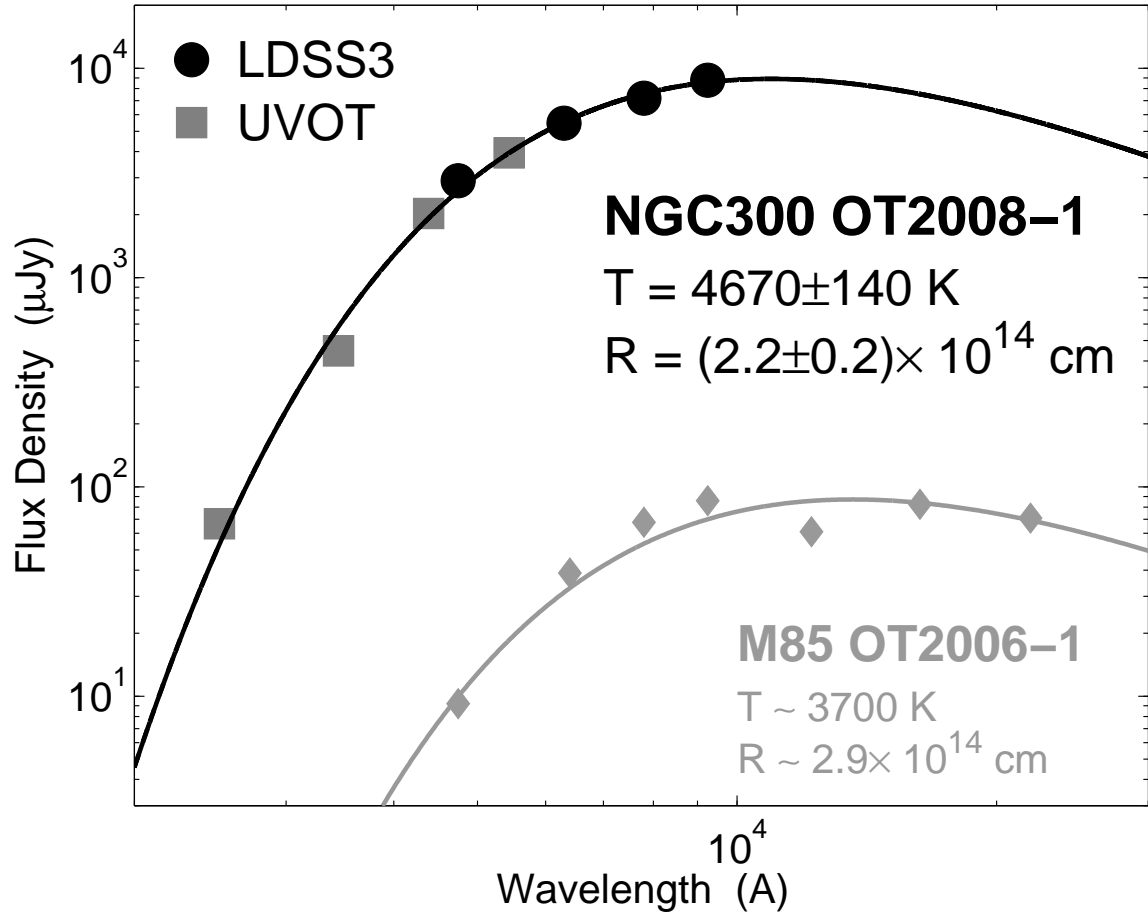


FIG. 1.— Optical (black circles) and UV (gray squares) spectral energy distribution of NGC 300 OT2008-1 on May 31.4 UT. *Swift*/UVOT data have been interpolated to this fiducial epoch using the observed decay rates (Table 2 and Figure 2). The black line is a blackbody model with the best-fit parameters,  $T = 4670 \pm 140$  K and  $R = (2.24 \pm 0.20) \times 10^{14}$  cm. Using an eruption date of April 17 UT, we find that the average expansion velocity of the outflow is about  $600 \text{ km s}^{-1}$ . Also shown is the SED for M85 OT2006-1 from Kulkarni et al. (2007), with an approximate blackbody model fit, indicating properties that closely match those of NGC 300 OT2008-1.

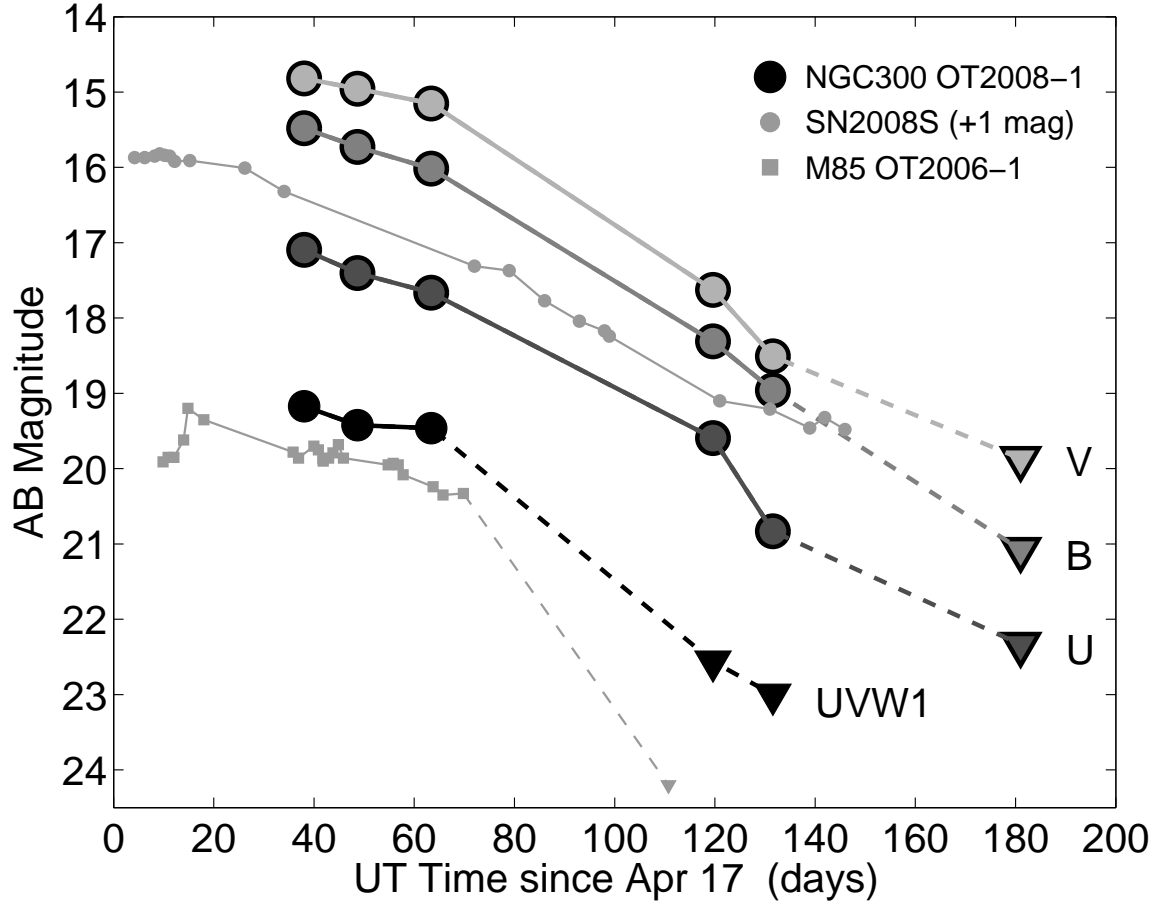


FIG. 2.— *Swift*/UVOT optical and UV light curves of NGC 300 OT2008-1 plotted relative to the fiducial eruption date of April 17 UT. The initial decay rate is about  $0.02 \text{ mag d}^{-1}$  for the first  $\sim 65$  d, followed by significant steepening at about 80–100 d. Also shown are the *R*-band light curves of SN 2008S (gray circles) and M85 OT2006-1 (gray squares). The temporal evolution of all three events is remarkably similar.

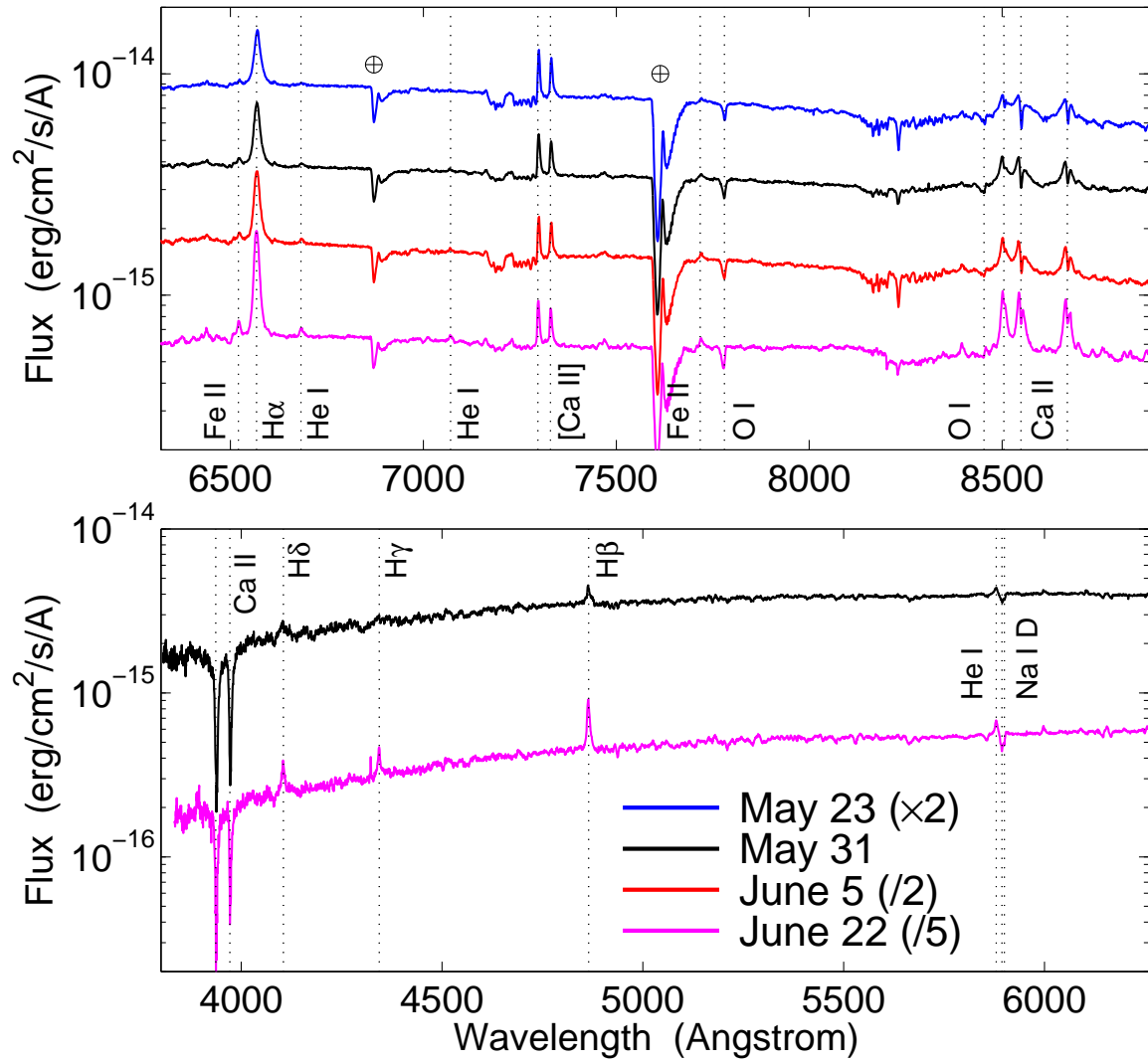


FIG. 3.— Low resolution spectra of NGC 300 OT2008-1 obtained with the LDSS-3 instrument on the Magellan/Clay 6.5-m telescope. *Top*: Red spectra with the dominant emission and absorption features identified. *Bottom*: Blue spectra with the dominant emission and absorption features identified.

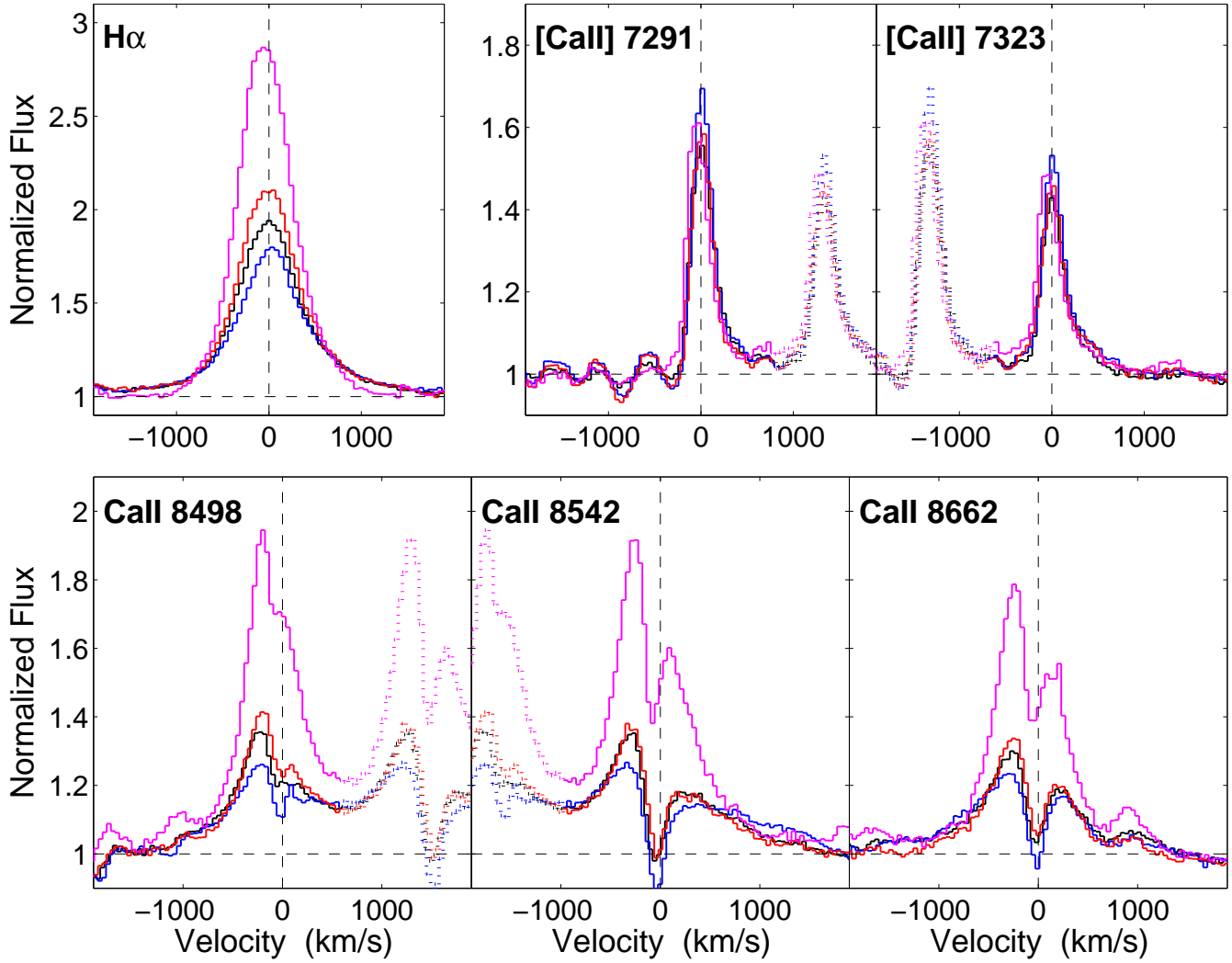


FIG. 4.— Velocity profiles of the dominant emission lines in the red low-resolution spectra obtained with LDSS-3 (line colors are as in Figure 3). The H $\alpha$  and Ca II IR triplet lines exhibit an increase relative to the continuum, while the [Ca II] lines remain largely unchanged.

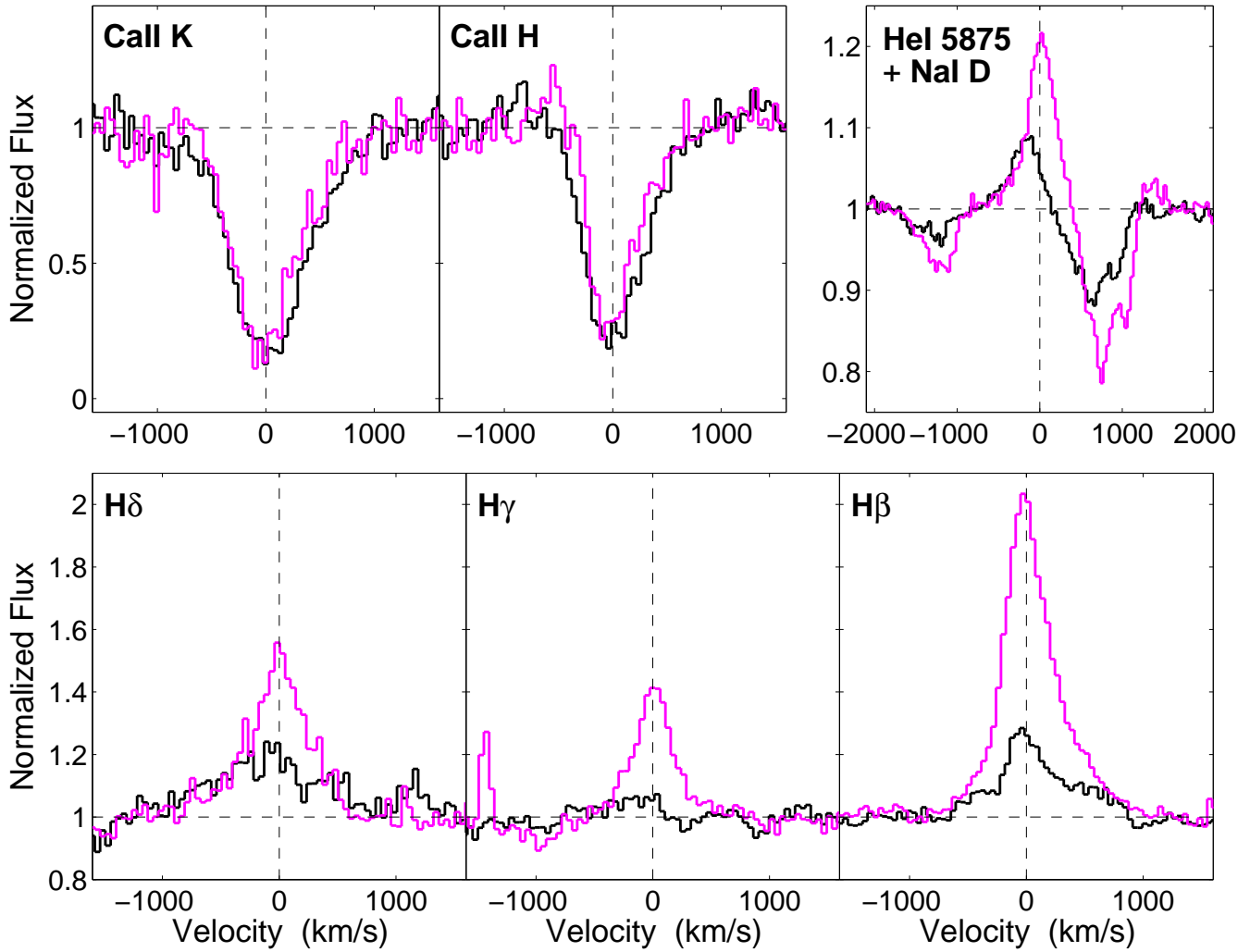


FIG. 5.— Velocity profiles of the dominant emission and absorption lines in the blue low-resolution spectra obtained with LDSS-3 (line colors are as in Figure 3). The Ca II H&K lines are somewhat narrower in the later spectrum, while the hydrogen Balmer lines and the He I  $\lambda$ 5877 line exhibit a significant increase relative to the continuum brightness. Similarly, the Na I D broad components exhibit increased absorption.

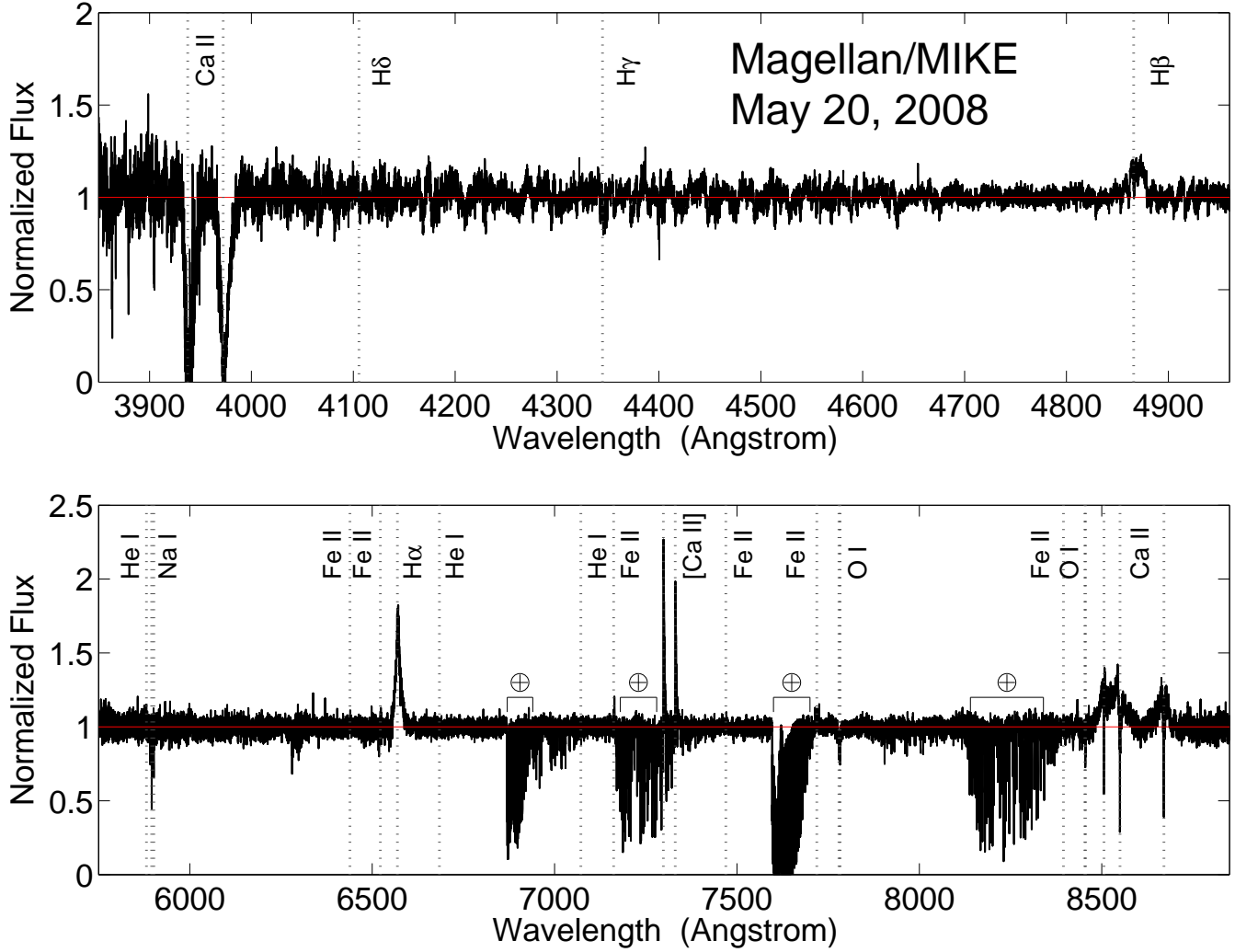


FIG. 6.— High resolution echelle spectrum of NGC 300 OT2008-1 obtained with the MIKE spectrograph mounted on the Magellan/Clay 6.5-m telescope on May 20.4 UT. The prominent lines are marked at a redshift of  $200 \text{ km s}^{-1}$ .

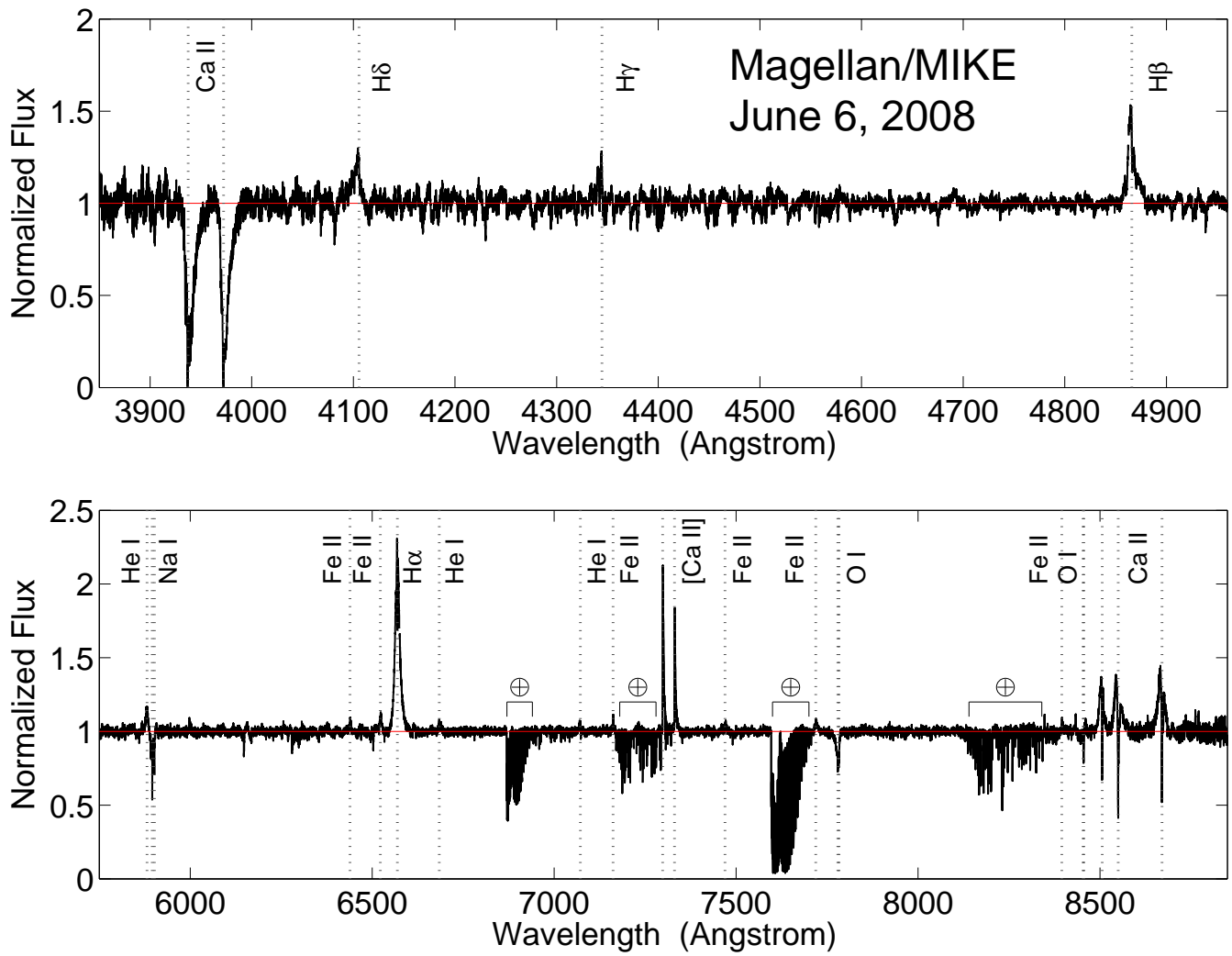


FIG. 7.— Same as Figure 6 but for a spectrum obtained on June 6.4 UT.

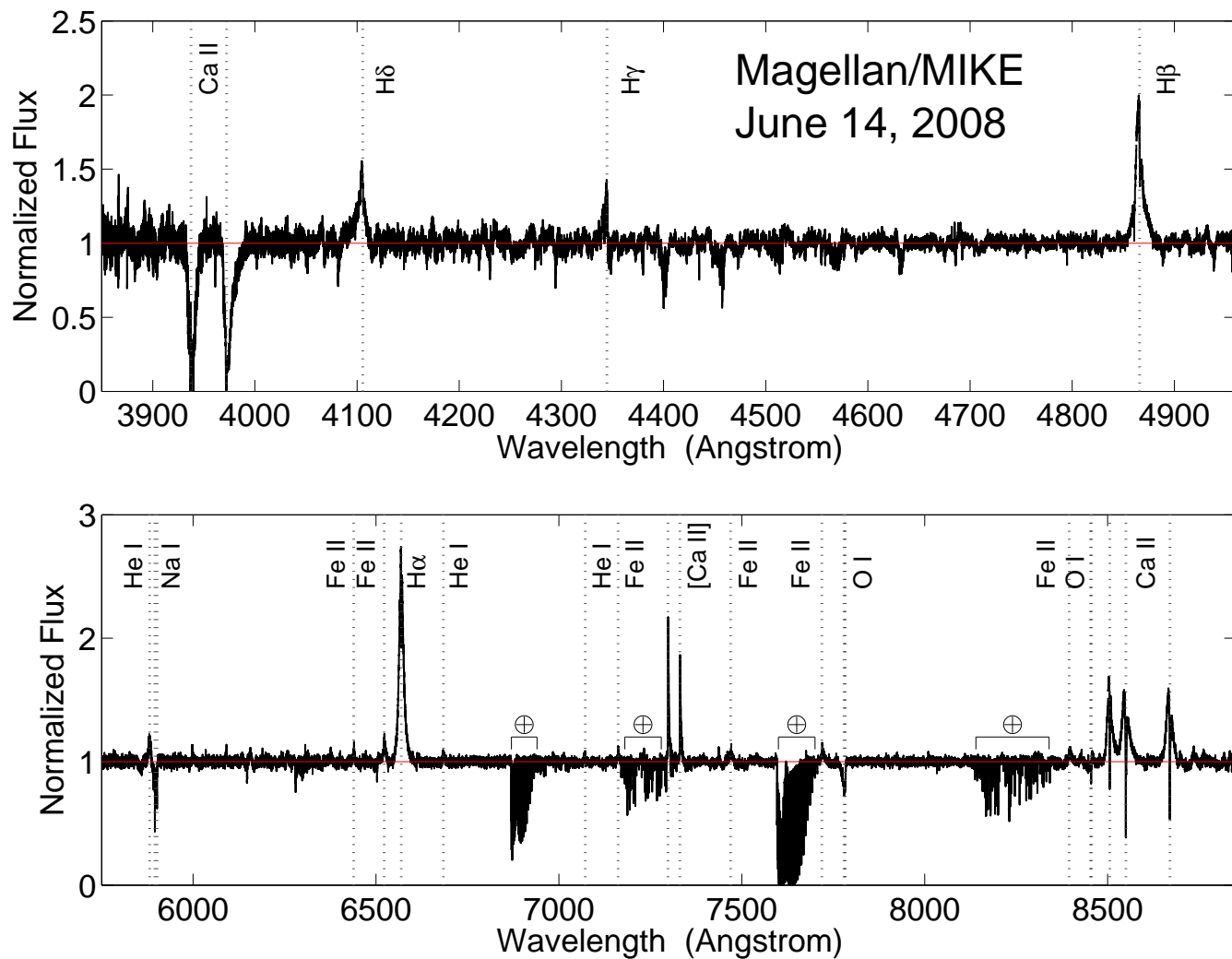


FIG. 8.— Same as Figure 6 but for a spectrum obtained on June 14.4 UT.

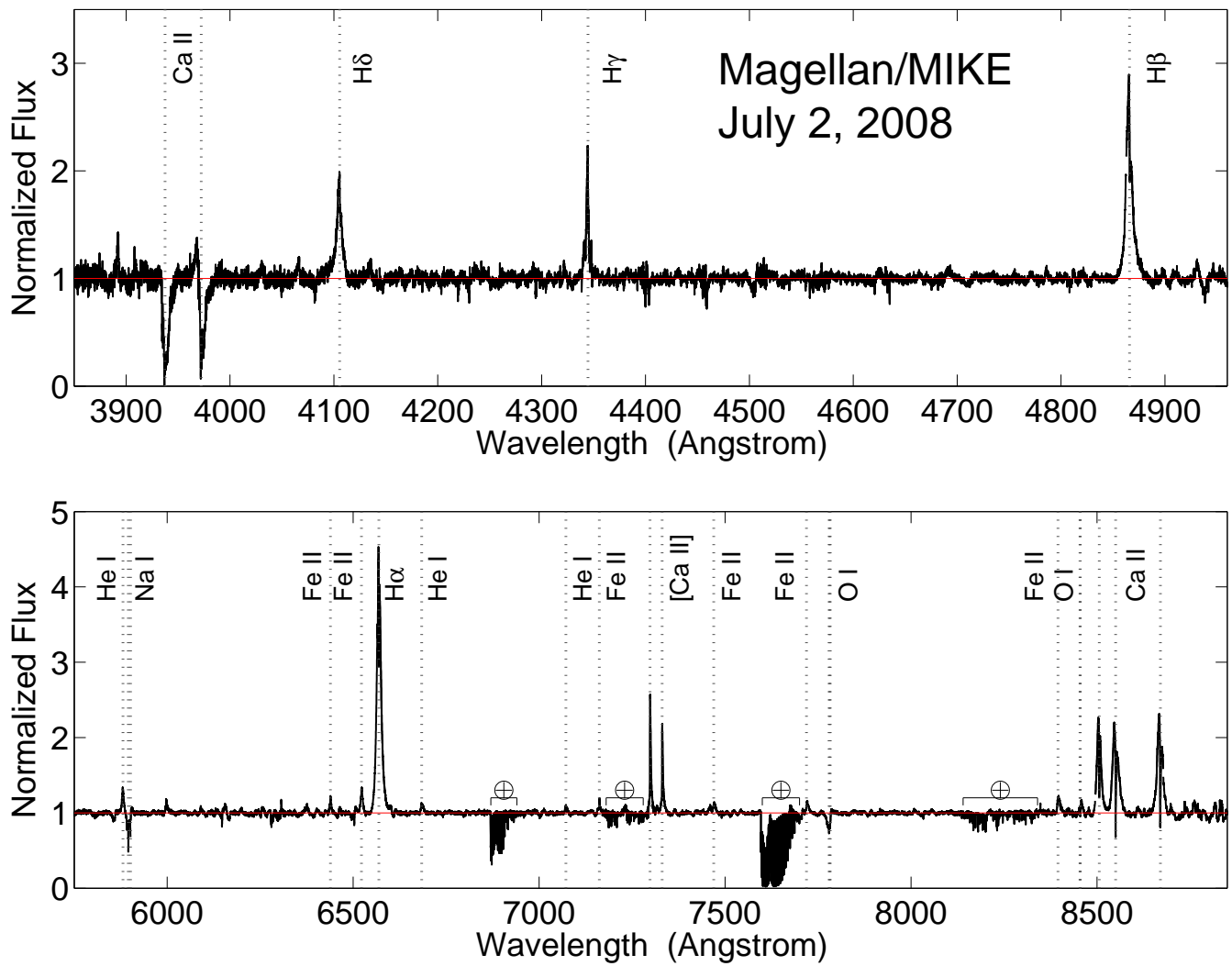


FIG. 9.— Same as Figure 6 but for a spectrum obtained on July 2.3 UT.

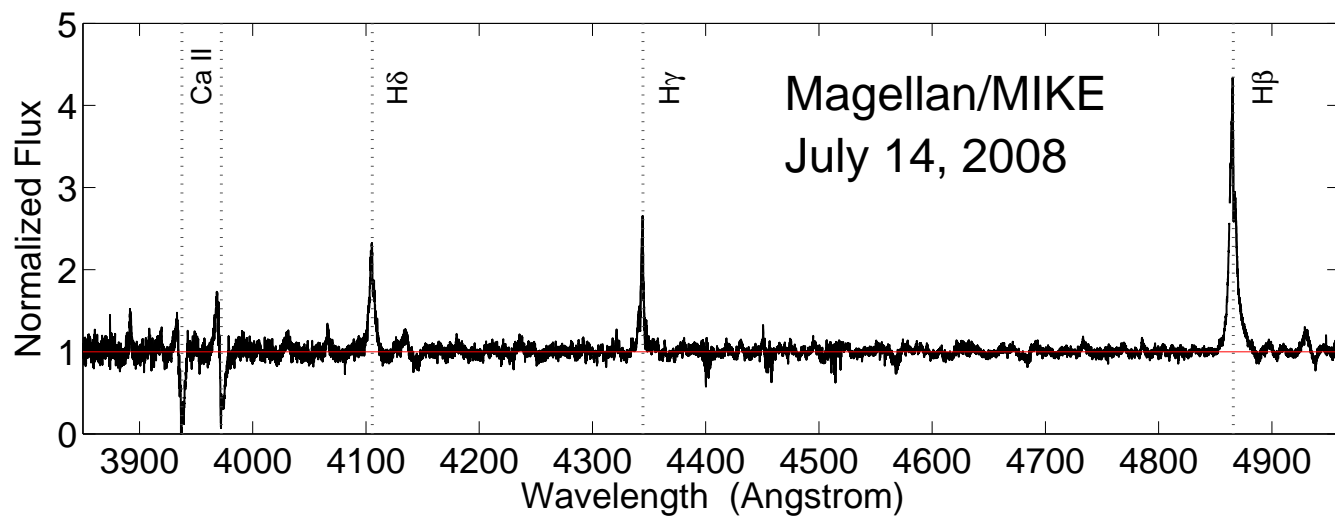


FIG. 10.— Same as Figure 6 but for a spectrum obtained on July 14.4 UT.

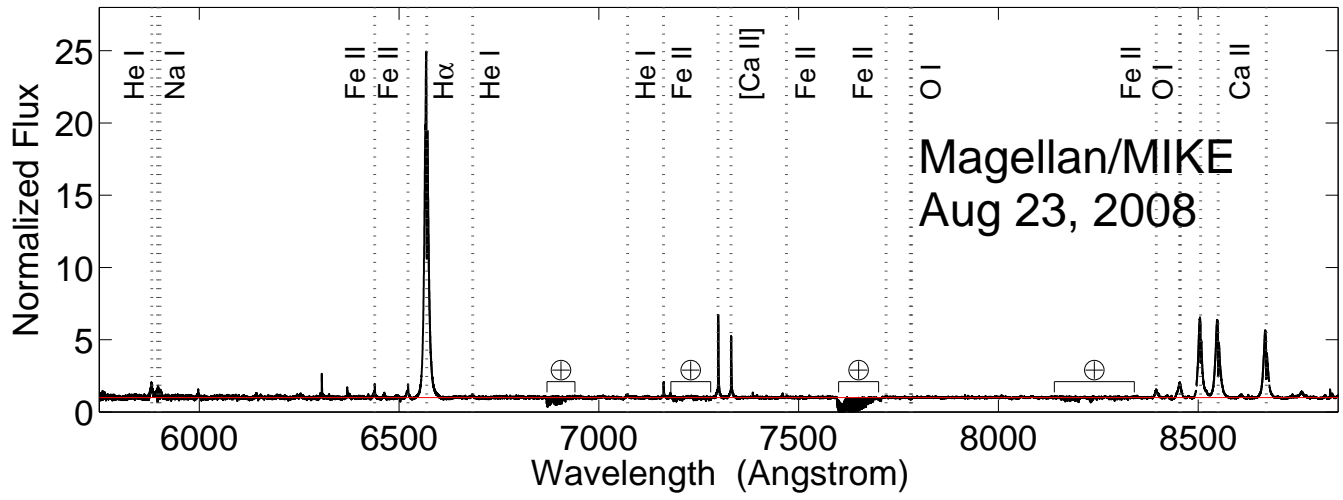


FIG. 11.— Same as Figure 6 but for a spectrum obtained on August 23.3 UT.

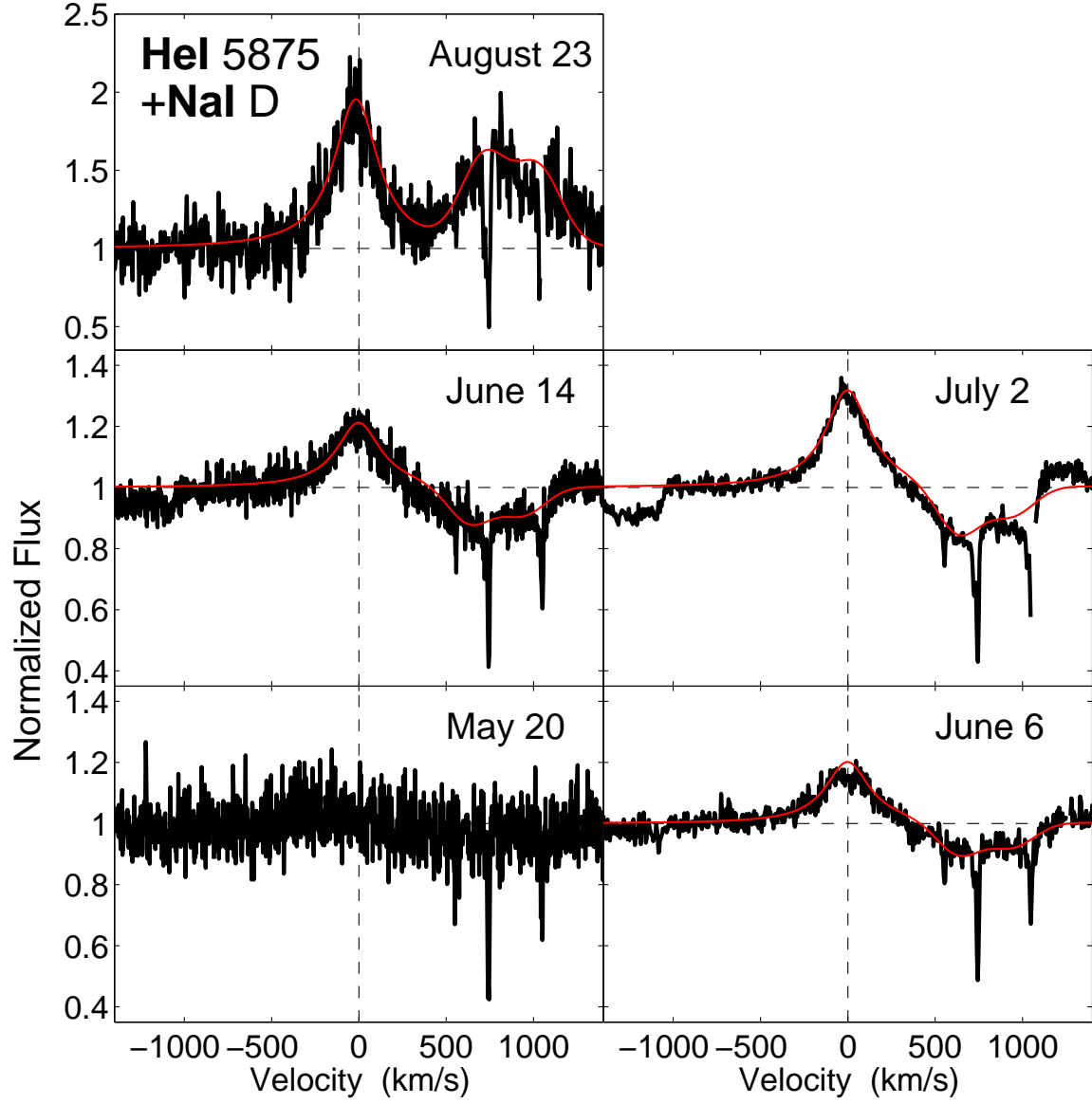


FIG. 12.— He I  $\lambda 5875$  and Na I D line profiles from the high-resolution spectra. The He I emission follows the same trend of increasing brightness relative to the continuum that is observed in other emission lines of NGC 300 OT2008-1 (e.g., Figure 17). The ion Na I D absorption exhibits both a narrow interstellar component and a wider component likely associated with the circumstellar environment. The broad component changes to emission in the final spectrum.

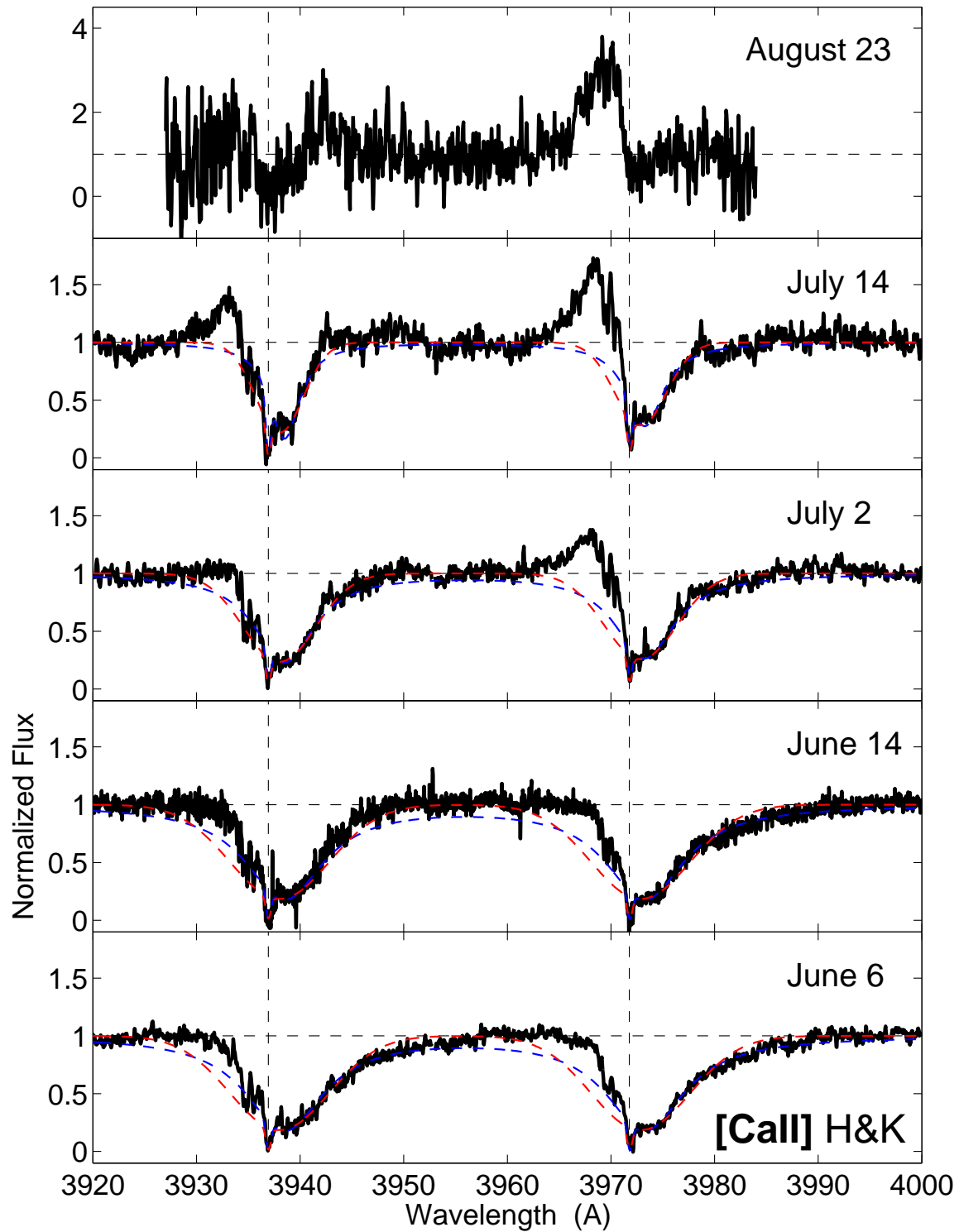


FIG. 13.— Absorption profiles of the Ca II H&K lines from the high-resolution spectra. Zero velocity is defined relative to the center of the narrow absorption component, and corresponds to a redshift of  $170 \text{ km s}^{-1}$ . The absorption features are broad and asymmetric, extending from about  $-400$  to  $+1100 \text{ km s}^{-1}$  on June 6 UT. The width of the red wing decreases with time, and the blue wing turns to emission. The dashed red and blue lines are, respectively, Lorentzian and Gaussian fits to the red wing of the lines.

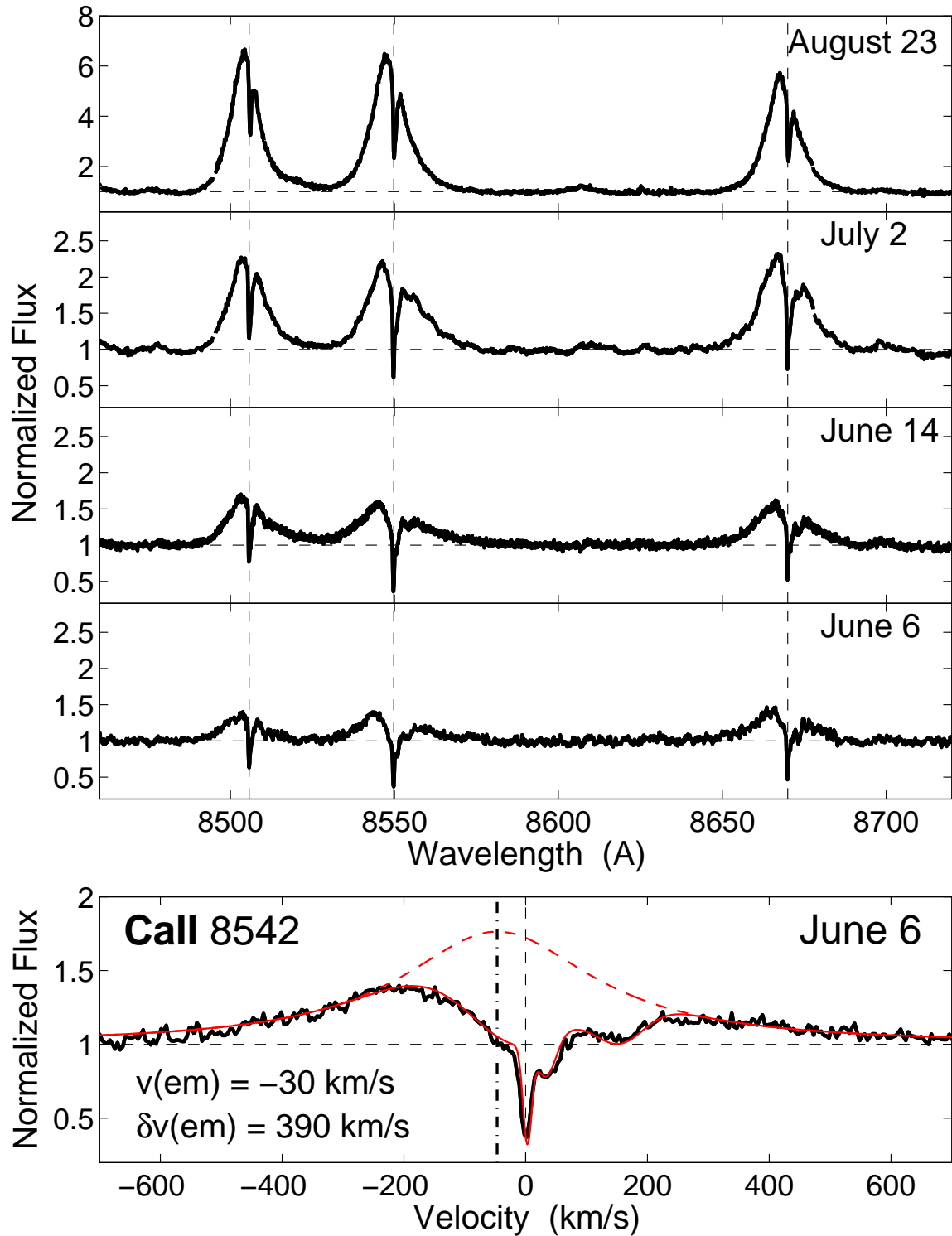


FIG. 14.— *Top*: Profiles of the Ca II IR triplet lines from the high-resolution spectra. *Bottom*: Zoom-in on the Ca II 8542 line from June 6. The solid red line is a combined model that includes a Lorentzian emission line (dashed red line; peak marked by dot-dashed blue line), absorbed by 4 distinct components: an interstellar unresolved component defining the zero velocity, and three broader absorption components that are all centered at velocities redshifted relative to the emission line center. The emission line center is blueshifted by about  $50 \text{ km s}^{-1}$  relative to the interstellar absorption.

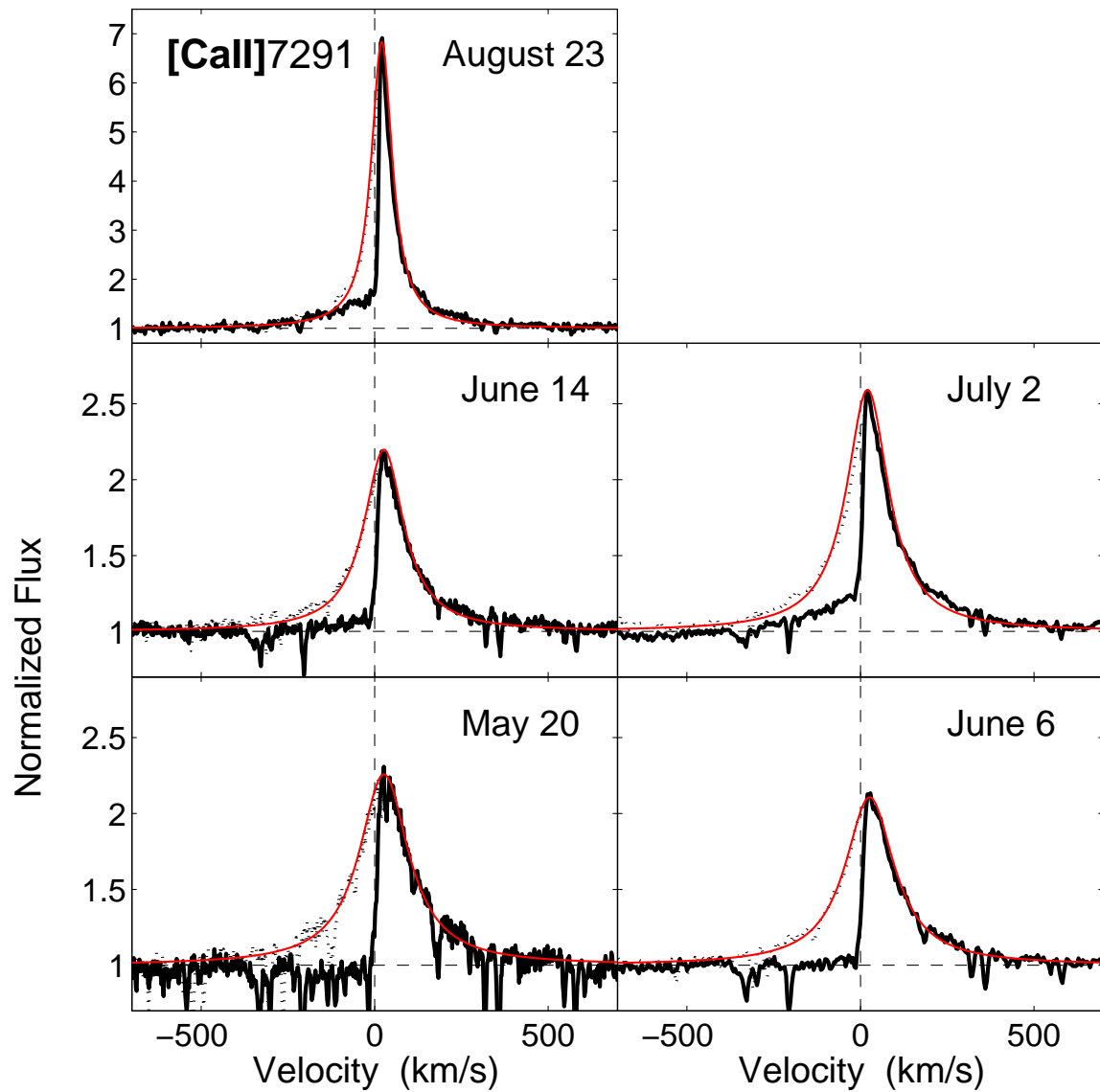


FIG. 15.— Emission lines of [Ca II]7291 from the high-resolution spectra. The lines are strongly asymmetric, with the blue wing of the line completely missing. A low level of blue-wing emission emerges on July 2, but it does not appear to brighten to the level of the red wing by August 23. The line width clearly decreases with time. The dotted black lines are a reflection of the red wing. The red lines are Lorentzian profile fits. The narrow absorption features in the various spectra are due to telluric lines.

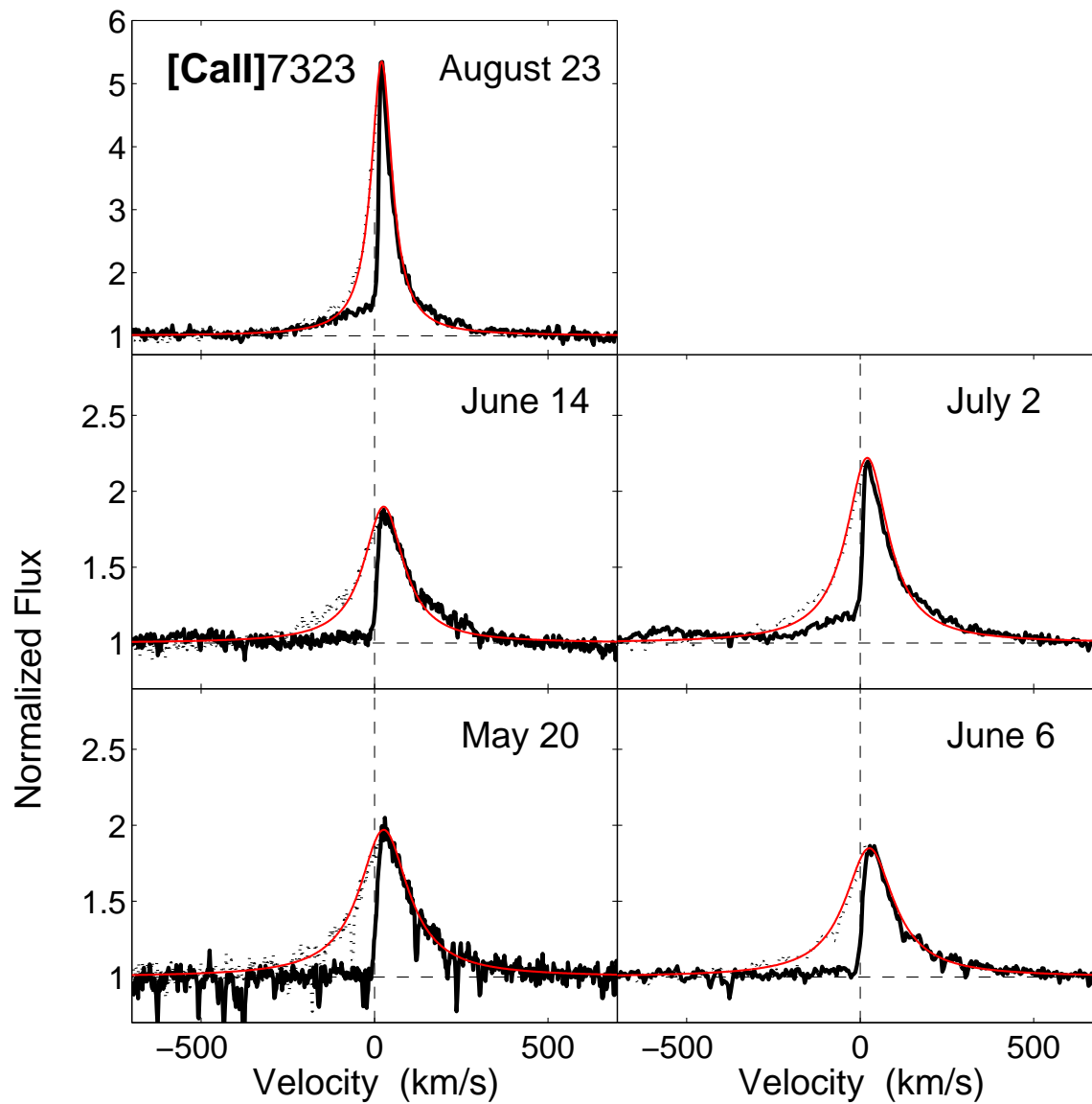


FIG. 16.— Same as Figure 15 but for the weaker [Ca II] 7323 line.

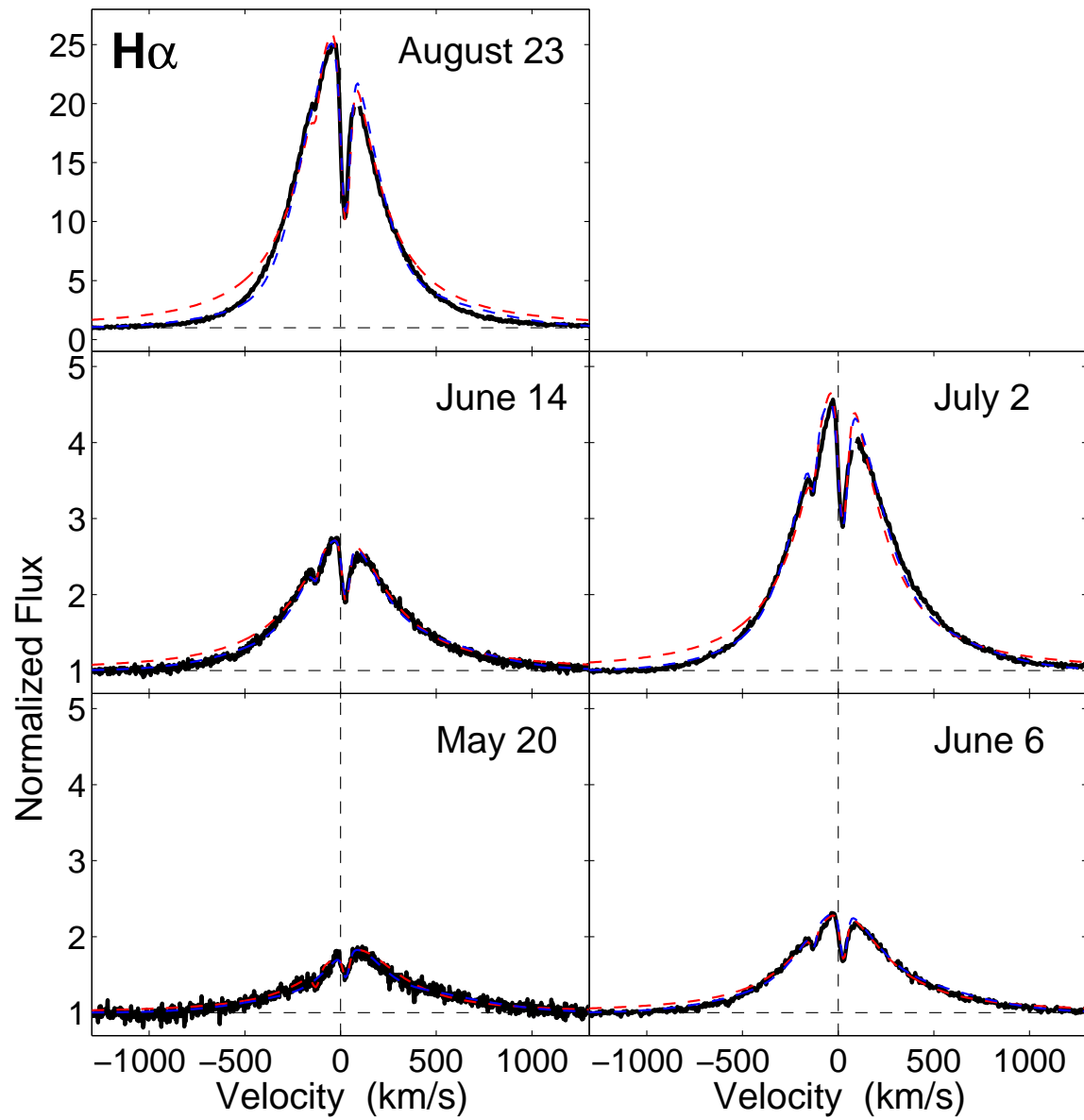


FIG. 17.—  $H\alpha$  emission lines from the high-resolution spectra. The lines are overall symmetric but are marked by a deep narrow absorption feature redward of the line center (a second absorption feature is possibly detected blueward of the line center). The dashed red lines are Lorentzian model fits, while the dashed blue lines are models with offset narrow and wide Gaussian components.

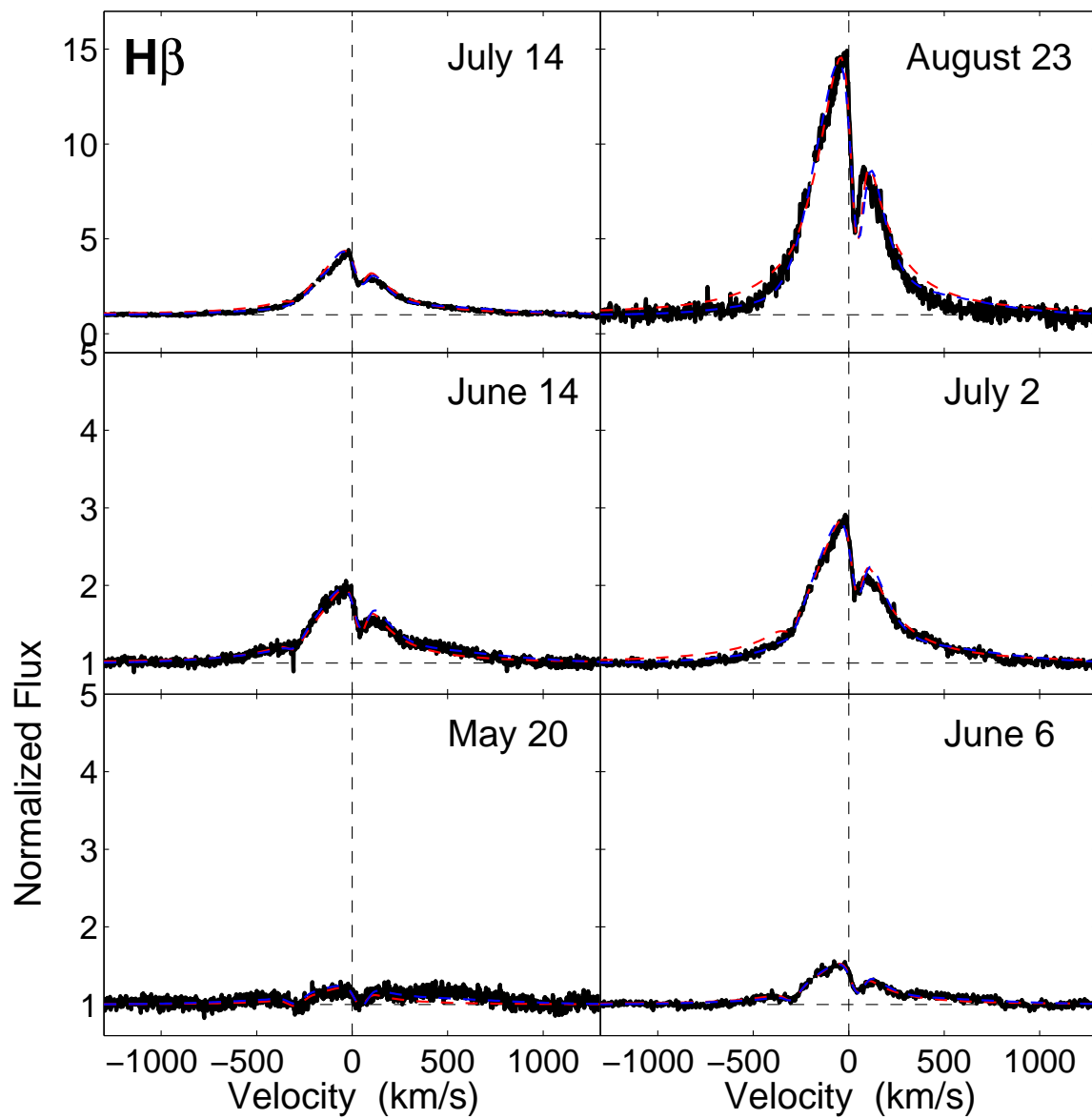


FIG. 18.— Same as Figure 17 but for the  $H\beta$  emission line.

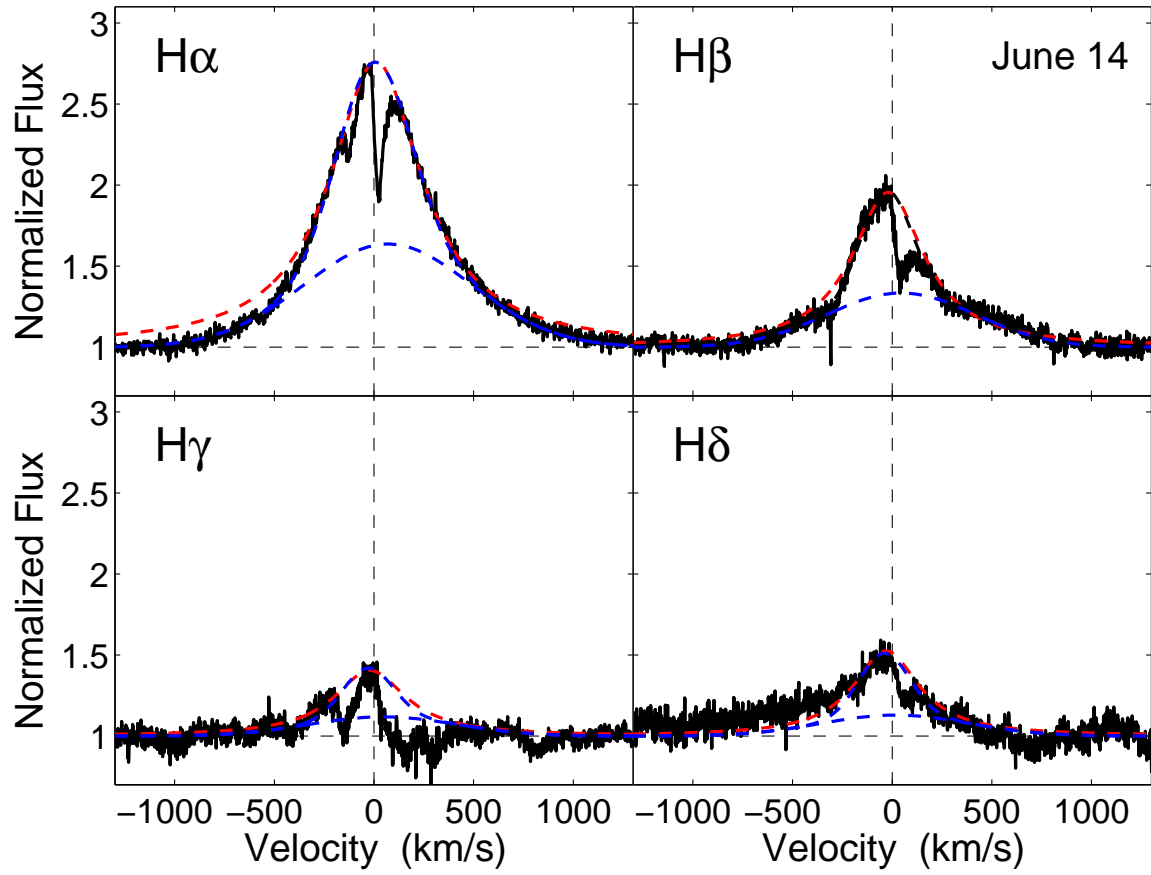


FIG. 19.— Hydrogen Balmer lines from the high resolution spectrum on June 14. The red and blue dashed lines are the same as in Figure 17, with the broad Gaussian component shown separately. We do not include the absorption features in these fits.

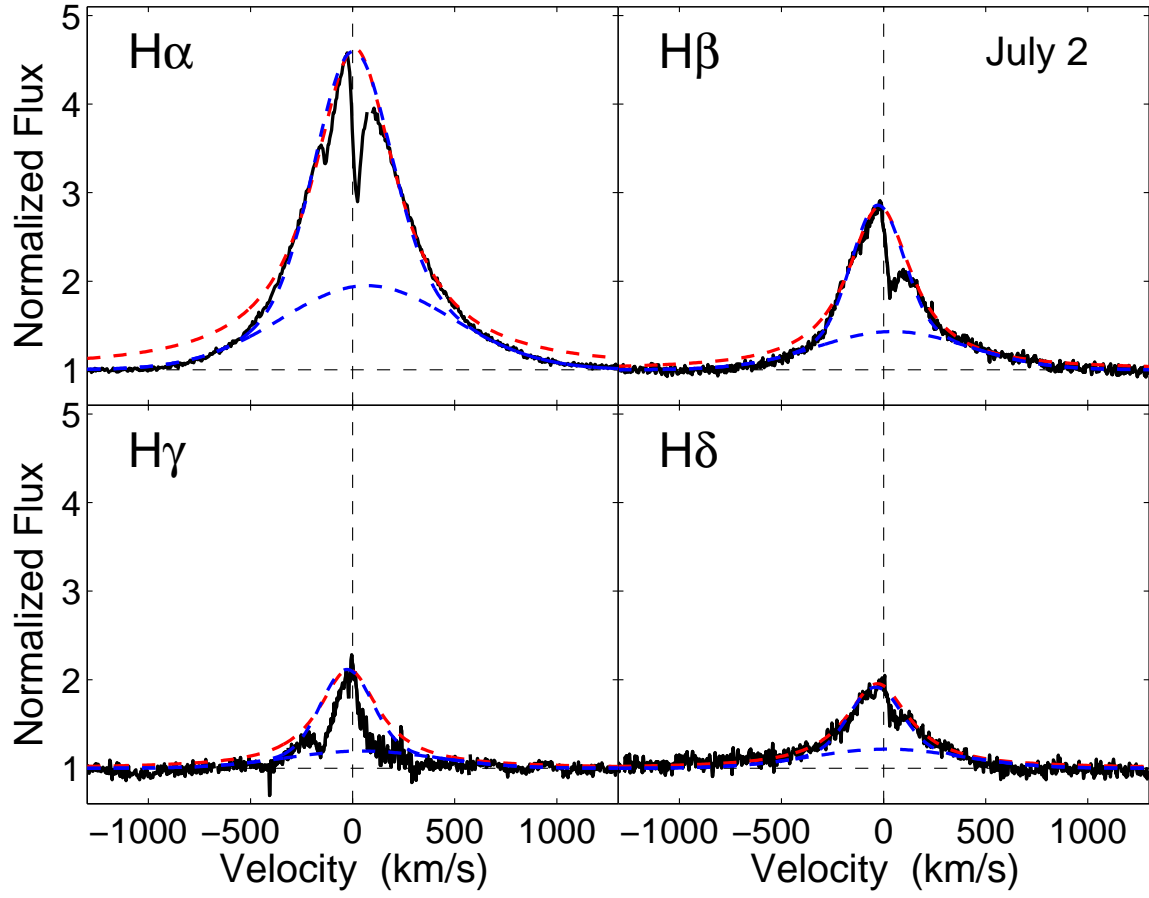


FIG. 20.— Same as Figure 19 but for the spectrum from July 2.

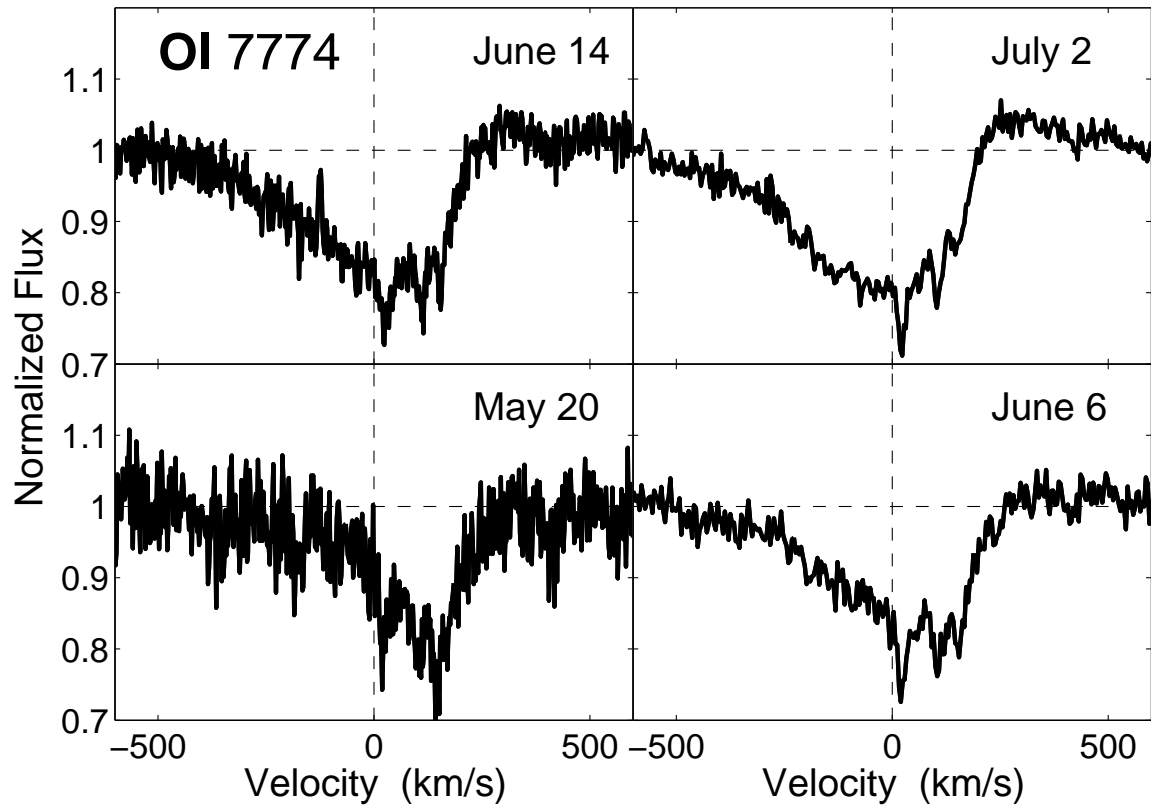


FIG. 21.— O I  $\lambda 7774$  triplet absorption profiles from the high-resolution spectra. The profiles are a combination of narrow interstellar components (clearly seen in the June 6, June 14, and July 2 spectra), and a broad component that is likely circumstellar in origin.

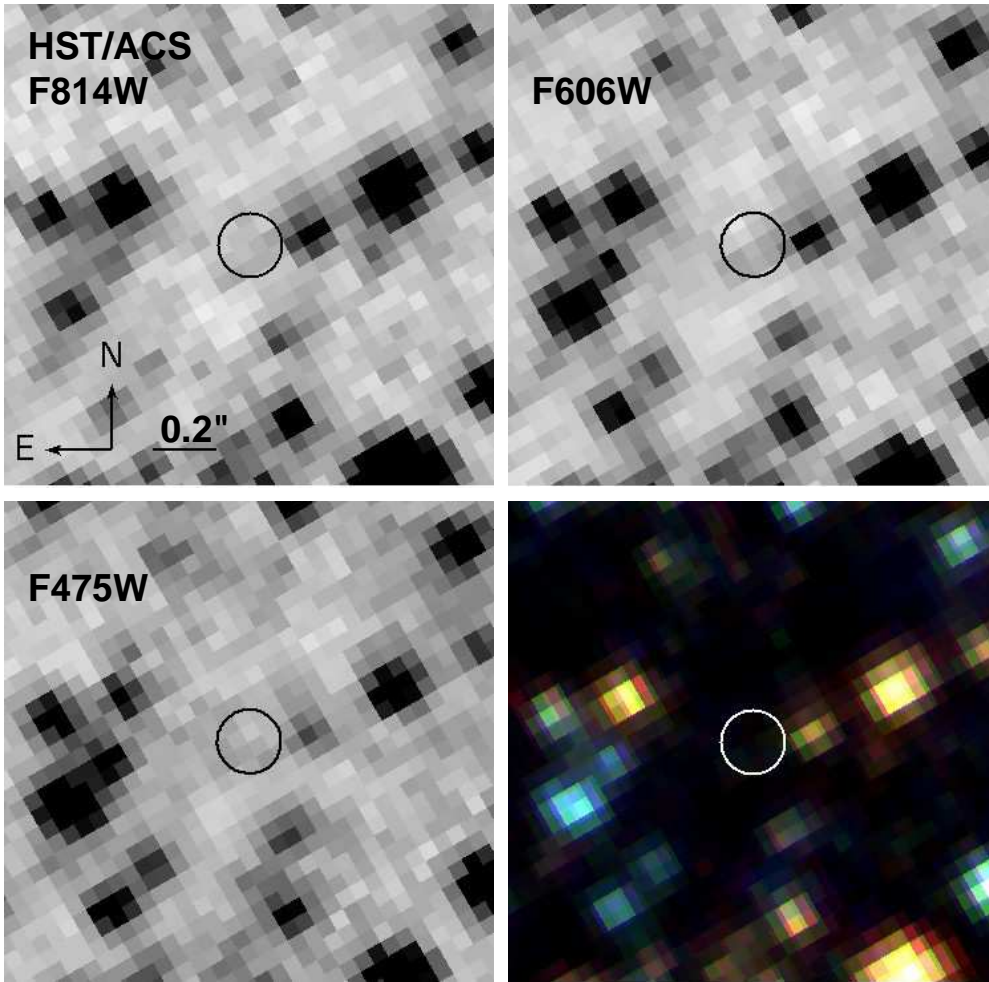


FIG. 22.— HST/ACS images at the location of NGC 300 OT2008-1 revealing no coincident source.

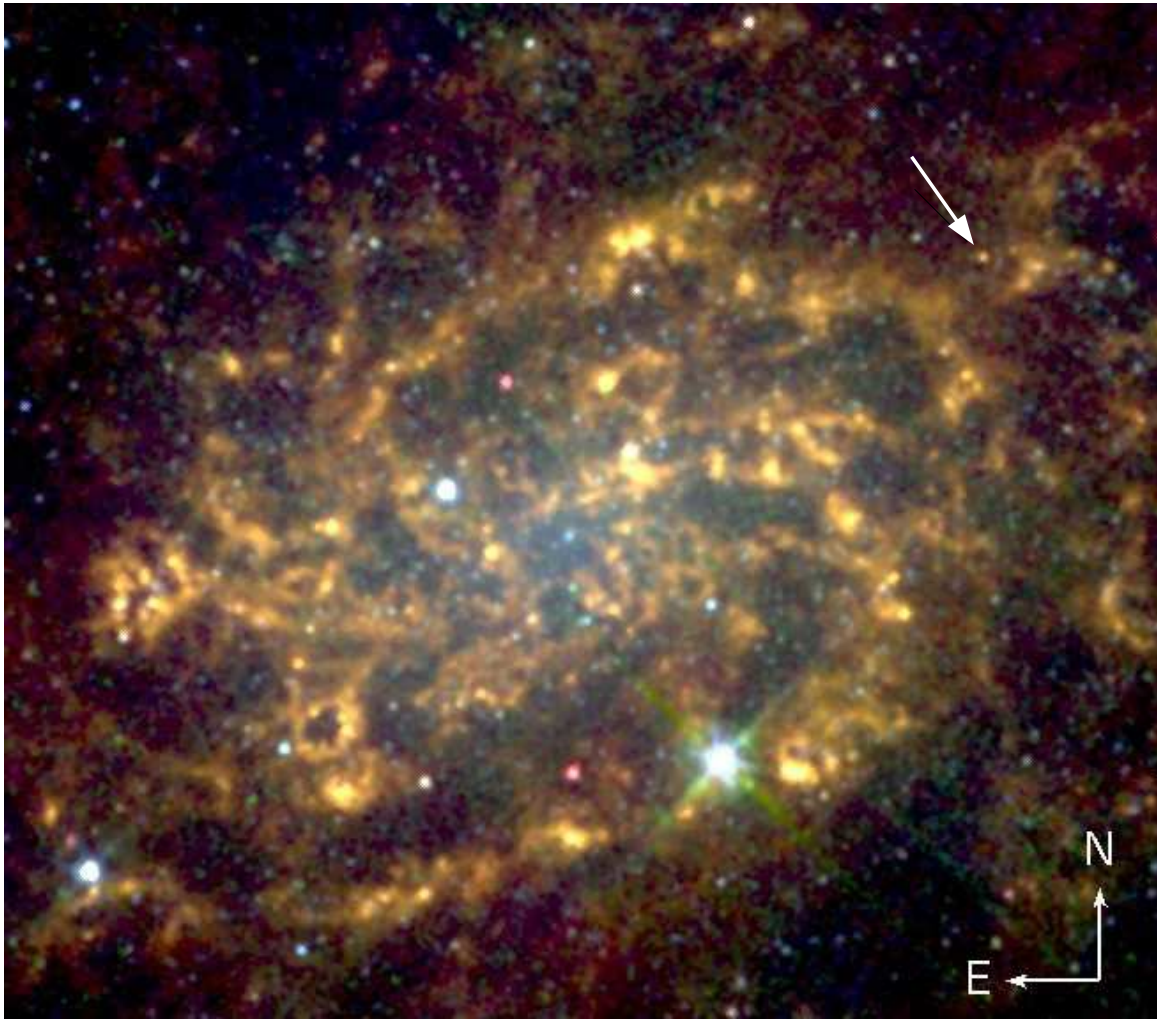


FIG. 23.— *Spitzer* false-color image of NGC 300 with the location of NGC 300 OT2008-1 marked by an arrow. The red, green, and blue channels correspond to the 4.5, 5.8 and 8.0  $\mu\text{m}$  IRAC images, respectively.

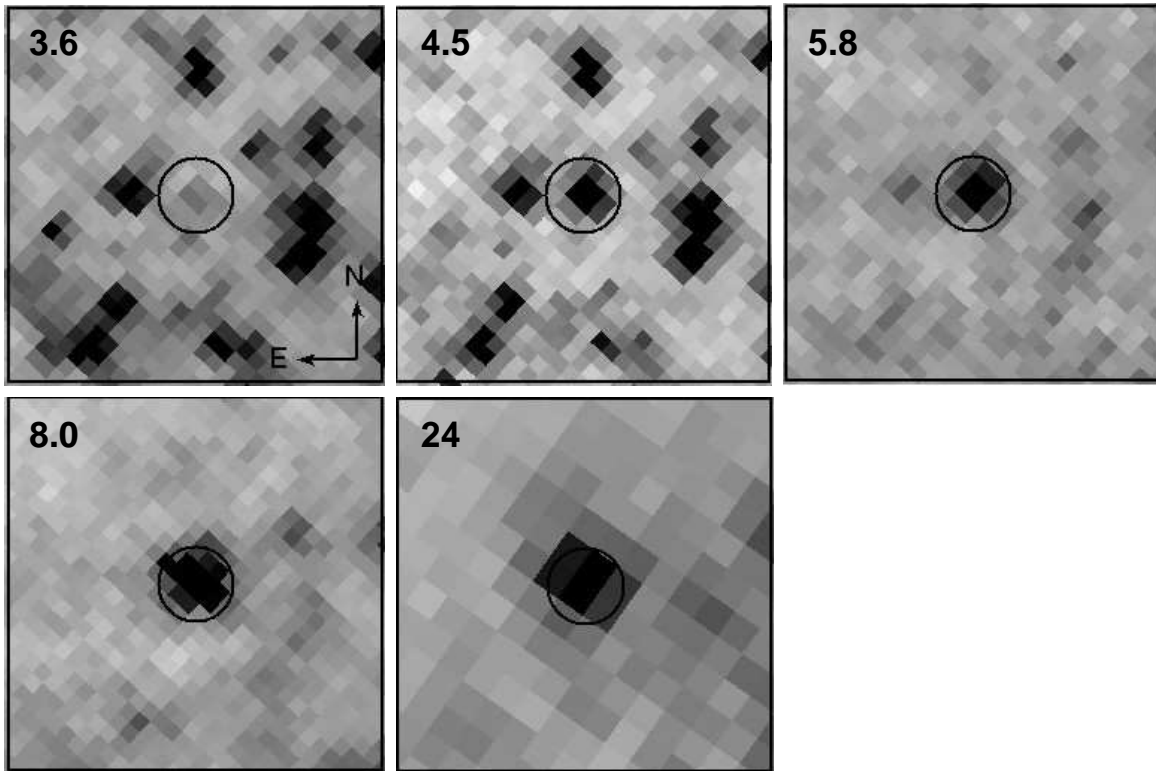


FIG. 24.— *Spitzer* IRAC and MIPS images of the progenitor of NGC 300 OT2008-1 from 3.6 to 24  $\mu\text{m}$ .

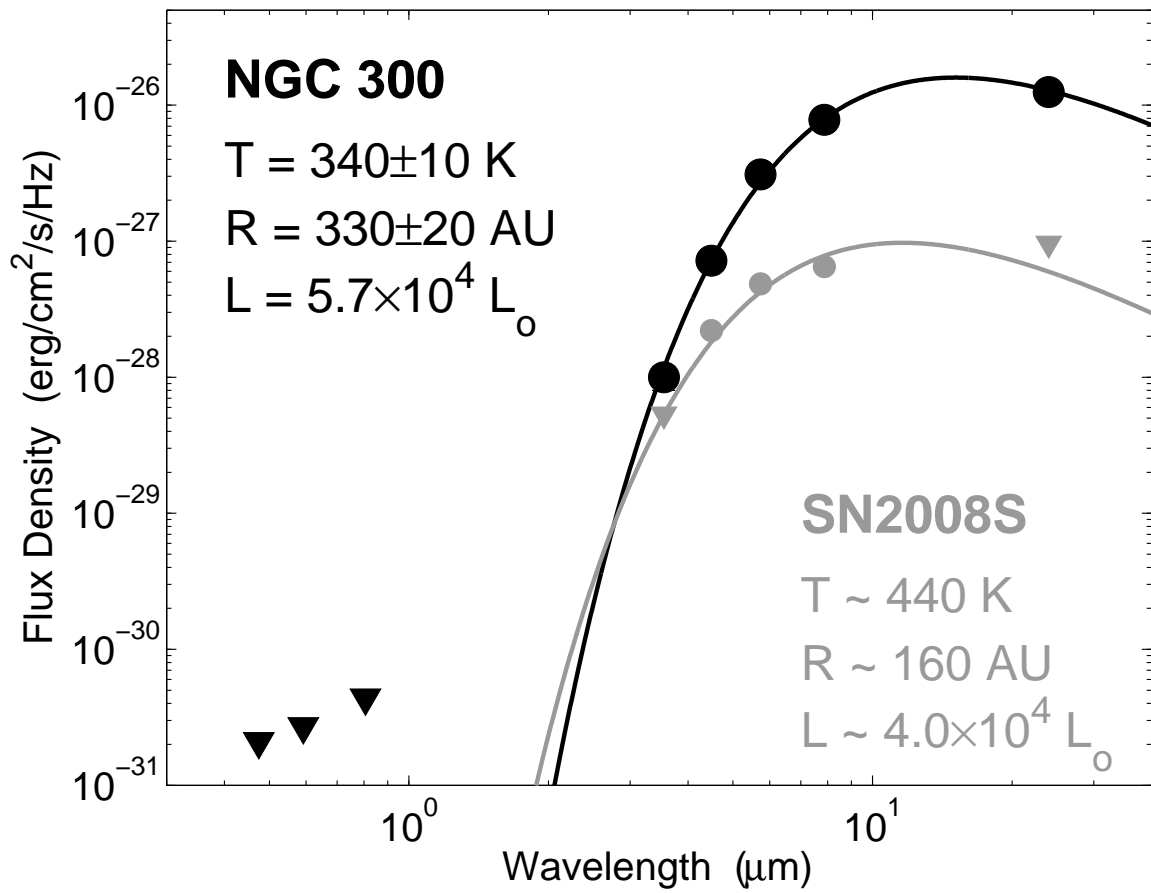


FIG. 25.— Spectral energy distribution of the archival source coincident with NGC 300 OT2008-1 from HST (upper limits) and *Spitzer* (black circles) observations. The black line is the best-fit blackbody model ( $\chi^2_r = 1.5$  for 3 degrees of freedom). Also shown is the SED of the *Spitzer* source coincident with SN 2008S (Prieto et al. 2008; Thompson et al. 2008) and its best-fit blackbody model. The two progenitors share similar properties.

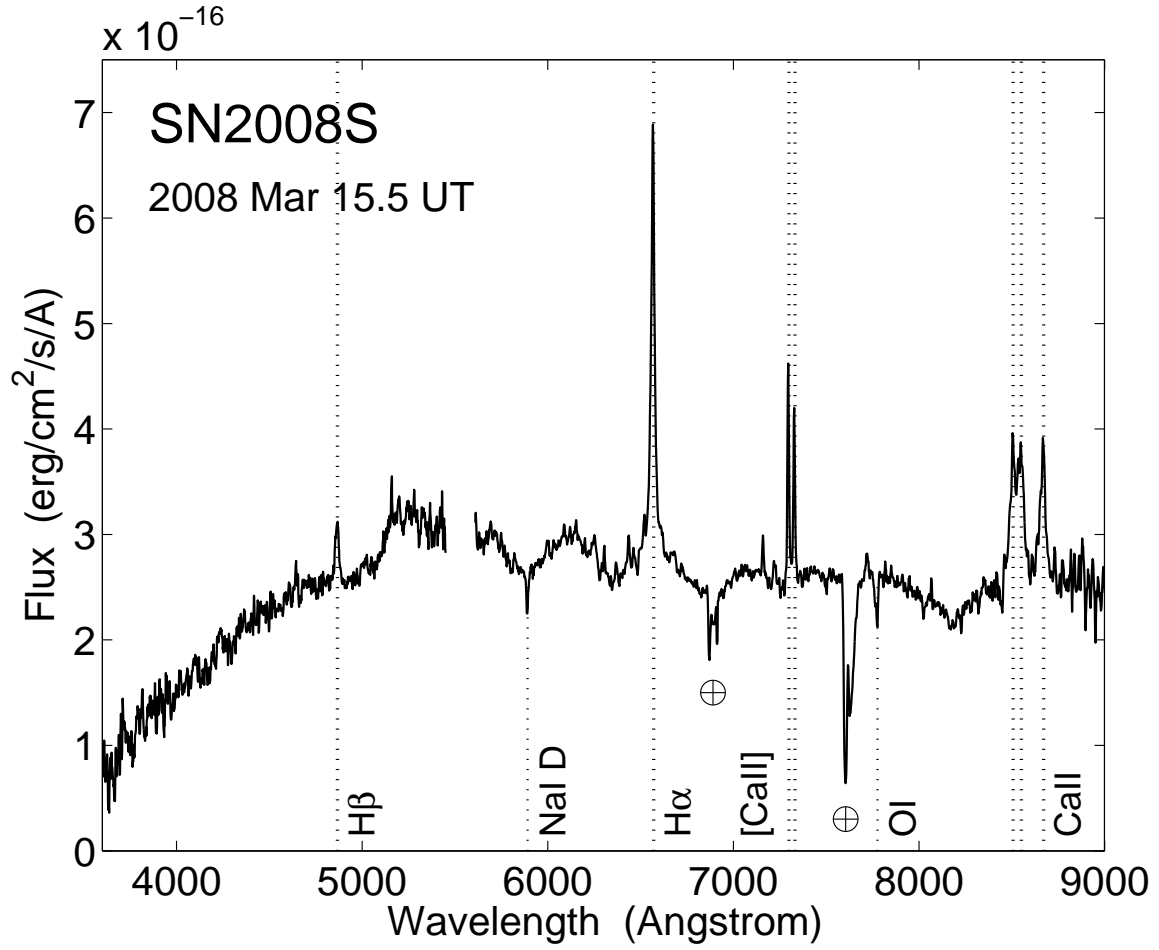


FIG. 26.— Low-resolution spectrum of SN2008S obtained with the ARC 3.5-m telescope at Apache Point Observatory about 42 d after discovery. The continuum shape and brightness, as well as the observed spectral features closely resemble those of NGC 300 OT2008-1, indicating that the two events likely share a common origin. We note, however, the lack of Ca II H&K absorption and He I emission, which are prominent in the spectrum of NGC 300 OT2008-1.